SPECTRAL METHODS SOLUTION OF THE NAVIER-STOKES EQUATIONS FOR STEADY VISCOUS FLOWS

A Dissertation by

German A. Vargas

Submitted to the Department of Mathematics and Statistics
and the faculty of the Graduate School of
Wichita State University
in partial fulfillment of
the requirements for the degree of
Doctor of Philosophy

May 2009

SPECTRAL METHODS SOLUTION OF THE NAVIER-STOKES EQUATIONS FOR STEADY VISCOUS FLOWS

The following faculty members have examined the final copy of this dissertation for form and content and recommend that it be accepted in partial fulfillment of the requirement for the degree of Doctor of Philosophy with a major in Applied Mathematics.

Alan Elcrat, Committee Chair

Kenneth Miller, Committee Member

Thomas DeLillo, Committee Member

Kirk Lancaster, Committee Member

Elizabeth Behrman, Committee Member

Accepted for the College of Liberal Arts and Sciences

William D. Bischoff

Accepted for the Graduate School

J. David McDonald
Associate Provost of Research and
Dean of the Graduate School

DEDICATION

To Diana

How can it be that mathematics, being after all a product of human thought independent of experience, is so admirably adapted to the objects of reality?

Albert Einstein

The profound study of nature is the most fertile source of mathematical discoveries.

Joseph Fourier

ACKNOWLEDGMENTS

I am grateful to God for giving me the opportunity to complete this project, he gave me commitment, motivation and patience when difficulties were arising.

I would like to thank my advisor Dr. Alan Elcrat for guiding me, keeping me always on track, and for being always available and willing to assist me.

I am grateful to my family,

to my wife Diana for her unconditional love and support in every step of my career, to my parents for believing in my skills and nourishing my curiosity since childhood, to my sister for her interest in my work and feeling happy and proud of my success, to my parents in law and all my cousins for making everything easier on me with their prayers.

I want to thank Tom Wallis for dedicating a computer for my computations and for his constant support. I also want to thank Janise, Terri, Deana and Mark for assisting me so many times in my career at WSU.

ABSTRACT

A combination of Spectral Methods and Finite Differences will be used to solve the Navier-Stokes equations for a viscous flow past a circular cylinder and past symmetric Joukowski airfoils. Different discretizations of the physical problem will be explored, and the solution of the equations will be analyzed for different geometries and boundary conditions.

This project is the continuation of our research started as a Master Thesis at Wichita State University under the advising of Professor Alan Elcrat; the project is a deep exploration of the solution of Navier-Stokes equations by implementing new methods of discretization including spectral differentiation. We will compare results previously obtained by Gauss-Seidel/Successive Over-Relaxation Methods (SOR) together with Finite Differences, with results using Newton's Method, based on work by Bengt Fornberg, but implementing spectral differentiation. As we will see, due to the nature of the physical domain and the conformal map involved to transform it to a more tractable domain, the use of spectral methods in both directions of our two dimensional problem proved to be inefficient due to unnecessary concentration of points in areas of the domain of low gradients. However, to take advantage of spectral methods, we combined spectral methods in one direction with high order finite

differences on the other direction, where different mesh densities were designed to have higher concentration of points where required. With this discretizations, spectral methods were approached as the limiting order of finite differences as presented in *A Practical Guide to Pseudospectral Methods* [14].

We will explore the solution for flows past more general geometries, symmetric Joukowski airfoils. Then we will study the implementation and effect of suction boundary conditions on the obstacle.

In this text I have decided to include part of the introduction and theoretical background shown in my Master thesis to allow new readers to get familiarized with the subject, but the solution scheme, the different discretizations and results are all new explorations that we are proud to present.

TABLE OF CONTENTS

Chapter **Page**

1 INTRODUCTION **1**

1.1 Historic Perspective 2

1.2 Partial Differential Equations 4

1.2.1 Equilibrium Problems 4

2 THEORETICAL BACKGROUND **6**

2.1 Equation of Continuity 7

2.2 Navier-Stokes Equation 9

3 MATHEMATICAL FORMULATION **12**

3.1 Stream Function and Vorticity 13

4 INTRODUCTION TO SPECTRAL METHODS **22**

5 DISCRETIZATION OF THE SYSTEM **25**

6 SOLUTION SCHEME **32**

7 BOUNDARY CONDITIONS **38**

7.1 Second Boundary condition on the Obstacle 41

TABLE OF CONTENTS

Chapter **Page**

8 STRUCTURE OF THE OPERATORS **45**

9 COMPUTATIONS **50**

10 Stream Function and Vorticity **54**

11 Drag Coefficient **65**

12 JOUKOWSKI TRANSFORMATION **69**

12.1 Case $x_c = 0.5$ 73

12.2 Case $x_c = 0.25$ 77

12.3 Case $x_c = 0.5$ for inverted airfoil 78

13 SUCTION BOUNDARY CONDITION **81**

14 CONCLUSIONS **85**

APPENDIX **88**

A PHYSICAL PROPERTIES OF SOME FLUIDS **89**

BIBLIOGRAPHY **90**

LIST OF FIGURES

Figure **Page**

4.1 Chebyshev collocation on the interval $[-1, 1]$ (see [13]) 23

5.1 Circular Cylinder in plane flow 25

5.2 Physical Domain (X Plane) 26

5.3 Mapped Domain (Z Plane) 26

5.4 Rectangular Grid in the Z Plane 27

5.5 Rectangular Grid mapped back to the X Plane 28

5.6 Chebyshev collocation in both ξ and η directions 29

5.7 Chebyshev collocation in the η direction and equispaced collocation in the ξ direction 30

5.8 Chebyshev collocation in the η direction and exponential collocation in the ξ direction 31

8.1 40×40 Differentiation matrix D_ξ 46

8.2 40×40 Differentiation matrix D_η 46

8.3 Structure of the operators $D_{\xi-\text{full}} = D_\xi \otimes I_\eta$ and $D_{\eta-\text{full}} = I_\xi \otimes D_\eta$ . . 47

8.4 Structure of the Laplacian 48

8.5 Structure of the Jacobian 48

LIST OF FIGURES

Figure **Page**

10.1 Stream Function for Potential Flow 54

10.2 Stream Function for Re=0.001 56

10.3 Vorticity for Re=0.001 56

10.4 Stream Function for Re=10 57

10.5 Stream Function (Closed Paths) for Re=15 57

10.6 Vorticity for Re=15 58

10.7 Close zoom to the obstacle. Vorticity for Re=15 58

10.8 Stream Function for Re=50 to Re=200 59

10.9 Stream Function for Re=250 to Re=500 60

10.10 Vorticity Function for Re=50 to Re=200. Contour levels shown: 0.1, 0.2, 0.3, 0.4, 0.5, 0.6, 0.7, 0.8, 0.9, 1, 1.2, 1.4, 1.6, 1.8, 2, 2.5, 3, 4, 5. . 61

10.11 Vorticity Function for Re=250 to Re=500. Contour levels shown: 0.1, 0.2, 0.3, 0.4, 0.5, 0.6, 0.7, 0.8, 0.9, 1, 1.2, 1.4, 1.6, 1.8, 2, 2.5, 3, 4, 5. . 62

10.12 Length of the wake vs. Reynolds number for R=20 to Re=130 63

10.13 Length and width of the wake vs. Reynolds number for R=20 to Re=550 64

LIST OF FIGURES

Figure **Page**

11.1 Vorticity value on the surface of the obstacle vs degrees from stagnation point 67

12.1 Physical Domain (X Plane) 70

12.2 Mapped Domain (Z Plane) 70

12.3 Rectangular grid in the Z Plane 71

12.4 Rectangular grid mapped back to the physical Z plane 71

12.5 Rectangular grid mapped back to the physical Z plane 74

12.6 Stream Function for Joukowski airfoil with $x_c = 0.5$ at Re=15 75

12.7 Vorticity for Joukowski airfoil with $x_c = 0.5$ at Re=15 75

12.8 Stream Function for Joukowski airfoil with $x_c = 0.5$ 76

12.9 Stream Function for Joukowski airfoil with $x_c = 0.25$ 77

12.10 Inverted Symmetric Joukowsky airfoils for $x_c = 0.5$ (top) and $x_c = 0.25$ (bottom) 78

12.11 Stream lines at $Re = 50$ for $x_c = 0.5$ (top) and $x_c = 0.25$ (bottom) . . 79

12.12 Stream lines at $Re = 50$ for $x_c = 0.5$ (top) and $x_c = 0.25$ (bottom) . . 80

LIST OF FIGURES

Figure **Page**

13.1 Stream function for Re=25 83

13.2 Stream function for Re=25, $K_{suction} = 10$ 83

13.3 Stream function for Re=25, $K_{suction} = 20$ 84

13.4 Stream function for Re=25, $K_{suction} = 80$ 84

13.5 Stream function for Re=25, $K_{suction} = -80$ 84

Chapter 1

INTRODUCTION

The equations that govern a fluid are very rich from several points of view. The non-linearity of the equations and the instability of the solutions give the problem great mathematical interest. The intrinsic difficulties to find the solution bring our skills and computational power to the edge. Physically, the complexity of the phenomena described, makes Computational Fluid Dynamics a complete interdisciplinary challenge.

Traditionally the understanding of the fluids was based on experimental and theoretical methods. The arrival of the digital computer and the development of the high speed personal computers have included a third method to attack fluid problems, the computational method.

The theoretical or analytical approach, and its exact solutions, is restricted to simple problems, with simple geometries, and is usually restricted to linear problems. The experimental approach is widely used for design of all types of machinery that involve fluids, but the tests are very expensive and are also physically limited to extreme conditions such as atmospheric reentry or any other high temperature or high velocity tests. On the other hand, the computational or numerical method, is sometimes able to overcome these restrictions, and the cost is very reduced compared to the experimental tests. However, the computational methods have their limitations like storage, speed, and sometimes an improper theoretical background to support the calculations.

1.1 Historic Perspective

One of the first important developments in CFD was the work by Richardson in 1910, introducing iterative schemes to solve Laplace's equation. Later, in 1918 an improved method was developed by Liebmann, in which differing from Richardson's values from both new and old iteration steps are used in each step, improving the convergence in the relaxation scheme. In 1928 the work of Courant, Friedrichs and Lewy, gave bases for advances in the study of uniqueness, existence and stability of

the solution of partial differential equations[2]. In 1933 A. Thom studied the flow past circular cylinders at low speed, from the numerical and experimental point of view. In his experimental observations, oscillations in the wake behind the cylinder gave rise to what is called the Karman Vortex Street even for low velocities of the fluid.[7] By 1955 Allen and Southwell attacked the problem of viscous flow past a cylinder, applying (by hand) Southwell's relaxation scheme. A year later G. K. Batchelor gave "A proposal concerning laminar wakes behind bluff bodies at large Reynolds numbers" in which from theoretical statements, he explores the possibility of closed wakes for high Reynolds numbers, and its implications.[6] A great development in this area was led by Bengt Fornberg who started to carry out computations in this area around 1980. By 1985 his research on steady viscous flow past a circular cylinder, was remarkably rich, solving the Navier-Stokes equations using Newton's Method to get a faster convergence and prevent time instabilities coming from the iteration process[8]. Our work in this project is based on his work, also using key concepts from his 1991 paper for a row of circular cylinders[10].

1.2 Partial Differential Equations

The majority of physical phenomena where the quantities involved change in space and time are governed by Partial Differential Equations, such as diffusion, electromagnetic wave propagation, determination of the spectrum in quantum mechanics and ***fluid mechanics***, among others. To fully understand the physical behavior of the models represented by these equations we need to have a clear mathematical understanding of the character and properties of the solutions of the governing equations. As we discussed, these equations can be solved analytically only for the simplest cases; to obtain quantitative results we need to make use of numerical methods.

1.2.1 Equilibrium Problems

Equilibrium or Boundary Value Problems are problems for which we need to find a solution of a partial differential equation on a closed domain restricted by a set of boundary conditions; sometimes they are also called "jury" problems, given that the boundary conditions are the jury of the solution of the PDE in the interior of the domain. These types of problems are governed by Elliptic partial differential equations, such as Laplace's Equation, Poisson's equation for the electrostatic potential, the time independent Schrödinger's equation, and of course, the steady Navier-Stokes

Equations.

The boundary conditions can be classified in three types: Dirichlet conditions where a fixed values is imposed for the solution in the boundary; Neumann conditions where the normal derivative of the solution is imposed in the boundary; and Robin conditions where we use a combination of Dirichlet and Neumann boundary conditions.[1],[2]

Chapter 2

THEORETICAL BACKGROUND

The phenomena treated in fluid mechanics is macroscopic, considering the fluid as a continuous medium. That is, no matter how small is the fluid element, it is always big enough to contain a large number of molecules. In this way, if we talk about infinitely small volume elements, we mean small elements compared with the volume of the body in consideration, but big compared with the distance between molecules.[4]

The involved quantities, as velocity, pressure, stream and vorticity will be expressed as functions of the coordinates, i.e. they make reference to the value of these quantities in a fixed point in the space.

The following is the derivation of the fundamental equations governing a fluid, starting with the equation expressing the conservation of matter.

2.1 Equation of Continuity

Let us consider a volume V_0 in space. The fluid mass contained in this volume is equal to

$$\int \rho \, dV \quad , \tag{2.1}$$

where ρ is the mass density of the fluid, and the integration is done over the volume V_0. The mass flowing per unit of time through the element of surface $\vec{df}$ is

$$\rho \vec{v} \cdot \vec{df} \quad . \tag{2.2}$$

The vector $\vec{df}$ has magnitude equal to the area of the element of surface, and its direction is normal to the element, taken outward by convention. Then, when $\rho \vec{v} \cdot \vec{df}$ is positive, the mass is flowing out from the volume, and is negative when the mass flows in the volume. The total mass flowing out the volume V_0 per unit of time is then:

$$\oint \rho \vec{v} \cdot \vec{df} \quad , \tag{2.3}$$

integrating over the complete surface enclosing the volume studied.

Now, the decrease of mass in the volume V_0 per unit of time is

$$-\frac{\partial}{\partial t}\int \rho \, dV \quad . \tag{2.4}$$

Equating these two expressions:

$$\frac{\partial}{\partial t}\int \rho \, dV = -\oint \rho \vec{v} \cdot \vec{df} \quad . \tag{2.5}$$

Transforming the surface integral into a volume integral via Stokes' Theorem:

$$\oint \rho \vec{v} \cdot \vec{df} = \int \nabla \cdot \rho \vec{v} \, dV \quad . \tag{2.6}$$

Then

$$\frac{\partial}{\partial t}\int \rho \, dV = -\int \nabla \cdot \rho \vec{v} \, dV \quad , \tag{2.7}$$

$$\int \left[\frac{\partial \rho}{\partial t} + \nabla \cdot \rho \vec{v}\right] dV = 0 \quad , \tag{2.8}$$

for any arbitrary volume, then, the integrand should be equal to zero:

$$\frac{\partial \rho}{\partial t} + \nabla \cdot \rho \vec{v} = 0 \quad . \tag{2.9}$$

This is the ***Equation of Continuity***, expressing that the density in a point in the space can change only due to a net flow of matter inward or outward.[4],[11]

2.2 Navier-Stokes Equation

Subsequently we will deduce the second fundamental equation of movement of a fluid:

Let us consider a volume in the fluid. The total force acting in this volume is equal to the integral of the pressure over the surface enclosing the volume,

$$-\oint P\, d\vec{f} \quad , \tag{2.10}$$

that can be transformed into a volume integral as,

$$-\oint P\, d\vec{f} = -\int \nabla P\, dV \quad . \tag{2.11}$$

That is, $-\nabla P$ is the force per unit of volume acting on the fluid.

We can now write the equation of movement of an element of volume in the fluid setting the force $-\nabla P$ equal to the product of the mass per unit of volume (ρ) times the acceleration:

$$\rho \frac{d\vec{v}}{dt} = -\nabla P \quad . \tag{2.12}$$

The derivative $\frac{d\vec{v}}{dt}$ in the previous equation, does not denote the change in the velocity of the fluid in a fixed point in space, but the change of the velocity of a given particle of the flow as it is moving in space. We need to express this derivative in terms of quantities referring to fixed points in space.

To achieve this, the change $d\vec{v}$ in the velocity of a given particle of the fluid over the time dt can be decomposed in two parts: the change over dt in the velocity of in a fixed point in space, and the difference between the velocities (in the same instant) of two points separated $d\vec{r}$, where $d\vec{r}$ is the distance traveled by the particle of the fluid during the time dt. The first part is

$$\left(\frac{\partial \vec{v}}{\partial t}\right) dt \quad , \tag{2.13}$$

where the derivative $\frac{\partial \vec{v}}{\partial t}$ is taken for a constant x, y, z value, that is, in a fixed point in the space.

The second part is

$$dx\frac{\partial \vec{v}}{\partial x} + dy\frac{\partial \vec{v}}{\partial y} + dz\frac{\partial \vec{v}}{\partial z} = (d\vec{r}\cdot\nabla)\,\vec{v} \quad . \tag{2.14}$$

Then,

$$d\vec{v} = \left(\frac{\partial \vec{v}}{\partial t}\right) dt + (d\vec{r}\cdot\nabla)\,\vec{v} \quad . \tag{2.15}$$

Dividing both sides by dt, we obtain

$$\frac{d\vec{v}}{dt} = \frac{\partial \vec{v}}{\partial t} + (\vec{v}\cdot\nabla)\,\vec{v} \quad . \tag{2.16}$$

Replacing $\frac{d\vec{v}}{dt}$ in (2.12), we have

$$\frac{\partial \vec{v}}{\partial t} + (\vec{v} \cdot \nabla)\, \vec{v} = -\frac{1}{\rho}\nabla P \quad . \tag{2.17}$$

Including not only external stresses like the pressure applied on the on volume element, but the shearing stresses, boundary layer theory [5] shows that the forces included in the shearing part of the stress tensor are related to the changes in velocity of the fluid by[2],[16]

$$\frac{\partial \vec{v}}{\partial t} + (\vec{v} \cdot \nabla)\, \vec{v} = -\frac{1}{\rho}\nabla P + \frac{\mu}{\rho}\nabla^2 \vec{v} \quad . \tag{2.18}$$

where μ is the coefficient of dynamic viscosity. Finally let $\nu = \frac{\mu}{\rho}$ be the kinematic viscosity, then we obtain

$$\frac{\partial \vec{v}}{\partial t} + (\vec{v} \cdot \nabla)\, \vec{v} = -\frac{1}{\rho}\nabla P + \nu\nabla^2 \vec{v} \quad . \tag{2.19}$$

This is the ***Navier-Stokes Equation*** for incompressible flow expressing the conservation of momentum, and shows that the velocity changes in response to convection $(\vec{v} \cdot \nabla)\, \vec{v}$, spatial variations in the pressure ∇P, and viscous forces $\nu\nabla^2 \vec{v}$, where ν is the kinematic viscosity, considered constant in this project. We are neglecting terms depending on the gravity (or other external forces) given that these are important just in large scale systems where the pressure changes as we increase the altitude.[4],[11]

Chapter 3

MATHEMATICAL FORMULATION

Our interest in this project is to study flows which do not depend on time. In this way, all the derivatives with respect to the time will be zero. Moreover we are assuming that the fluid is incompressible, having constant density over the fluid (this is a good approximation under the condition of subsonic flow).[4]

In general, the pressure is given in terms of the density and the temperature through the state equation. When the temperature changes, an additional equation for the conservation of the energy is required. For this project we will assume that the temperature is constant in the fluid.

Under these conditions, the equations (2.9) and (2.19) are transformed to

$$\nabla \cdot \vec{v} = 0 \quad , \tag{3.1}$$

$$(\vec{v} \cdot \nabla)\, \vec{v} = -\frac{1}{\rho}\nabla P + \nu \nabla^2 \vec{v} \quad . \tag{3.2}$$

For a two dimensional flow, these equations can be written explicitly in terms of the x and y components of the velocity, denoted by u and v respectively, as:

$$\frac{\partial u}{\partial x} + \frac{\partial v}{\partial y} = 0 \quad , \tag{3.3}$$

$$u\frac{\partial u}{\partial x} + v\frac{\partial u}{\partial y} = -\frac{1}{\rho}\frac{\partial P}{\partial x} + \nu \nabla^2 u \quad , \tag{3.4}$$

$$u\frac{\partial v}{\partial x} + v\frac{\partial v}{\partial y} = -\frac{1}{\rho}\frac{\partial P}{\partial y} + \nu \nabla^2 v \quad . \tag{3.5}$$

3.1 Stream Function and Vorticity

This system of three coupled non-linear equations can be solved directly, but for a problem in two dimensions it is more convenient to replace the velocity field by two

equivalent scalar fields[3],[18],[20]: the stream function $\psi(x, y)$, and the vorticity $\zeta(x, y)$. We define the ***stream function*** ψ as:

$$u = \frac{\partial \psi}{\partial y} \qquad ; \qquad v = -\frac{\partial \psi}{\partial x} \quad . \tag{3.6}$$

Where we introduce the concept of (*streamline*) as a curve whose tangent at any point is the velocity at that point.

For steady flow, the streamlines are time invariant and coincide with the path of the particles; we can say also that the mass flow perpendicular to this line is zero.

This definition for the stream function is a convenient way to satisfy the equation of continuity (3.3)

$$\frac{\partial u}{\partial x} + \frac{\partial v}{\partial y} = \frac{\partial^2 \psi}{\partial x \partial y} - \frac{\partial^2 \psi}{\partial x \partial y} = 0 \quad . \tag{3.7}$$

From

$$(\vec{v} \cdot \nabla)\, \psi = 0 \quad , \tag{3.8}$$

is shown that $\vec{v}$ is tangent to the lines of ψ constant, that is, tangent to the streamlines, which can be verified easily as follows:

$$(\vec{v}\cdot\nabla)\,\psi = \left(u\frac{\partial}{\partial x} + v\frac{\partial}{\partial y}\right)\psi = u\frac{\partial\psi}{\partial x} + v\frac{\partial\psi}{\partial y} = u\,(-v) + v\,(u) = 0 \quad . \tag{3.9}$$

The ***vorticity*** is defined by

$$\zeta = \frac{\partial u}{\partial y} - \frac{\partial v}{\partial x} \quad , \tag{3.10}$$

which is equivalent to

$$\zeta = -curl(\vec{v}) = -\left(\nabla\times\vec{v}\right) = \frac{\partial u}{\partial y} - \frac{\partial v}{\partial x} \quad . \tag{3.11}$$

From (3.6), we can see that the vorticity ζ is related to the stream function ψ by the expression:

$$\zeta = \frac{\partial u}{\partial y} - \frac{\partial v}{\partial x} = \frac{\partial^2\psi}{\partial y^2} + \frac{\partial^2\psi}{\partial x^2} \quad . \tag{3.12}$$

Then:

$$\nabla^2\psi = \zeta \quad . \tag{3.13}$$

We can obtain an equation for ζ from the derivative of (3.4) with respect to y

$$\frac{\partial u}{\partial y}\frac{\partial u}{\partial x} + u\frac{\partial^2 u}{\partial x\partial y} + \frac{\partial v}{\partial y}\frac{\partial u}{\partial y} + v\frac{\partial^2 u}{\partial y^2} = -\frac{1}{\rho}\frac{\partial^2 P}{\partial x\partial y} + \nu\frac{\partial\left(\nabla^2 u\right)}{\partial y} \quad . \tag{3.14}$$

Analogously, differentiating (3.5) with respect to x,

$$\frac{\partial u}{\partial x}\frac{\partial v}{\partial x}+u\frac{\partial^2 v}{\partial x^2}+\frac{\partial v}{\partial x}\frac{\partial v}{\partial y}+v\frac{\partial^2 v}{\partial x\partial y}=-\frac{1}{\rho}\frac{\partial^2 P}{\partial x\partial y}+\nu\frac{\partial\left(\nabla^2 v\right)}{\partial x} \quad . \tag{3.15}$$

Now, subtracting the two previous equations we obtain

$$\frac{\partial u}{\partial x}\underbrace{\left(\frac{\partial u}{\partial y}-\frac{\partial v}{\partial x}\right)}_{\zeta}+u\left(\frac{\partial^2 u}{\partial x\partial y}-\frac{\partial^2 v}{\partial x^2}\right)+\frac{\partial v}{\partial y}\underbrace{\left(\frac{\partial u}{\partial y}-\frac{\partial v}{\partial x}\right)}_{\zeta}+$$

$$v\left(\frac{\partial^2 u}{\partial y^2}-\frac{\partial^2 v}{\partial x\partial y}\right)=\nu\left[\frac{\partial\left(\nabla^2 u\right)}{\partial y}-\frac{\partial\left(\nabla^2 v\right)}{\partial x}\right] \quad , \tag{3.16}$$

$$\frac{\partial u}{\partial x}\zeta+u\left(\frac{\partial^2 u}{\partial x\partial y}-\frac{\partial^2 v}{\partial x^2}\right)+\frac{\partial v}{\partial y}\zeta+v\left(\frac{\partial^2 u}{\partial y^2}-\frac{\partial^2 v}{\partial x\partial y}\right)=\nu\left[\frac{\partial\left(\nabla^2 u\right)}{\partial y}-\frac{\partial\left(\nabla^2 v\right)}{\partial x}\right] \tag{3.17}$$

Replacing u and v from the definition of Stream Function and using the equation of continuity

$$\zeta\ \underbrace{\frac{\partial u}{\partial x}+\frac{\partial v}{\partial y}}_{\frac{\partial^2\psi}{\partial x\partial y}-\frac{\partial^2\psi}{\partial x\partial y}=0}+\frac{\partial\psi}{\partial y}\underbrace{\left(\frac{\partial^2 u}{\partial x\partial y}-\frac{\partial^2 v}{\partial x^2}\right)}_{\frac{\partial\zeta}{\partial x}}-\frac{\partial\psi}{\partial x}\underbrace{\left(\frac{\partial^2 u}{\partial y^2}-\frac{\partial^2 v}{\partial x\partial y}\right)}_{\frac{\partial\zeta}{\partial y}}$$

$$=\nu\left[\frac{\partial\left(\nabla^2 u\right)}{\partial y}-\frac{\partial\left(\nabla^2 v\right)}{\partial x}\right] \quad , \tag{3.18}$$

$$\frac{\partial\psi}{\partial y}\frac{\partial\zeta}{\partial x}-\frac{\partial\psi}{\partial x}\frac{\partial\zeta}{\partial y}=\nu\left[\frac{\partial\left(\nabla^2 u\right)}{\partial y}-\frac{\partial\left(\nabla^2 v\right)}{\partial x}\right] \quad , \tag{3.19}$$

and

$$\nu\left[\frac{\partial\left(\nabla^2 u\right)}{\partial y}-\frac{\partial\left(\nabla^2 v\right)}{\partial x}\right]=\nu\left[\frac{\partial}{\partial y}\left(\frac{\partial^2 u}{\partial x^2}+\frac{\partial^2 u}{\partial y^2}\right)-\frac{\partial}{\partial x}\left(\frac{\partial^2 v}{\partial x^2}+\frac{\partial^2 v}{\partial y^2}\right)\right] \quad . \tag{3.20}$$

Then

$$\frac{\partial\psi}{\partial y}\frac{\partial\zeta}{\partial x}-\frac{\partial\psi}{\partial x}\frac{\partial\zeta}{\partial y}=\nu\nabla^2\underbrace{\left(\frac{\partial u}{\partial y}-\frac{\partial v}{\partial x}\right)}_{\zeta} \quad . \tag{3.21}$$

Finally we obtain

$$\nu\nabla^2\zeta=\frac{\partial\psi}{\partial y}\frac{\partial\zeta}{\partial x}-\frac{\partial\psi}{\partial x}\frac{\partial\zeta}{\partial y} \quad . \tag{3.22}$$

In this treatment we are considering all the quantities to be nondimensional variables; where the velocities are measured in terms of the velocity of the fluid at infinity U_∞, the distances are measured in terms of the size of the obstacle (half of the diameter L of the circle in our case) $L/2$. We can relate each of the variables to its corresponding physical quantities (not normalized versions with subscript p) by:

$$u=\frac{u_p}{U_\infty}\ , \qquad v=\frac{v_p}{U_\infty}\ , \qquad x=\frac{x_p}{L/2}\ , \qquad y=\frac{y_p}{L/2}\ , \qquad P=\frac{P_p}{\rho U_\infty}$$

If we want to relate the results with physical fluids it is enough to multiply the distances by the speed of the flow at infinity U_∞ and the distances by $L/2$. In our

previous equation the units for the vorticity will cancel form both sides of the equation but the laplacian will have units of length squared in the denominator, therefore we need to divide by $(L/2)^2$. The right hand side must be multiplied by U_∞ due to $\frac{\partial \psi}{\partial y}$ and $\frac{\partial \psi}{\partial x}$ which correspond to velocities and also divide by $L/2$ due to the denominator of $\frac{\partial \zeta}{\partial x}$ and $\frac{\partial \zeta}{\partial y}$. Leading to the following equation in physical coordinates (ignoring the subscript p):

$$\frac{4\nu}{L^2}\nabla^2\zeta = \frac{2U_\infty}{L}\left[\frac{\partial \psi}{\partial y}\frac{\partial \zeta}{\partial x} - \frac{\partial \psi}{\partial x}\frac{\partial \zeta}{\partial y}\right] \quad . \tag{3.23}$$

Rearranging

$$\nabla^2\zeta = \frac{U_\infty L}{2\nu}\left[\frac{\partial \psi}{\partial y}\frac{\partial \zeta}{\partial x} - \frac{\partial \psi}{\partial x}\frac{\partial \zeta}{\partial y}\right] \quad , \tag{3.24}$$

And recall from chapter 2 that the relation between kinematic viscosity ν and dynamic viscosity μ is given by $\nu = \frac{\mu}{\rho}$, then our previous equation can be written as

$$\nabla^2\zeta = \frac{Re}{2}\left[\frac{\partial \psi}{\partial y}\frac{\partial \zeta}{\partial x} - \frac{\partial \psi}{\partial x}\frac{\partial \zeta}{\partial y}\right] \quad . \tag{3.25}$$

Where $Re = U_\infty \rho L/\mu$ is the Reynolds number, a non-dimensional quantity, named in honor to the British physicist Osborne Reynolds. This number represents the relation between the inertial and viscous forces. If the number is close to zero, the

inertial forces can be neglected compared to the viscous forces. If the number is large (10^{10}), the viscous forces can be neglected.[3],[21]

Now, we can find an equation relating the pressure; differentiating (3.4) with respect to x

$$\left(\frac{\partial u}{\partial x}\right)^2 + u\frac{\partial^2 u}{\partial x^2} + \frac{\partial v}{\partial x}\frac{\partial u}{\partial y} + v\frac{\partial^2 u}{\partial x \partial y} = -\frac{1}{\rho}\frac{\partial^2 P}{\partial x^2} + \nu\frac{\partial\left(\nabla^2 u\right)}{\partial x} \quad , \tag{3.26}$$

and differentiating (3.5) with respect to y

$$\frac{\partial u}{\partial y}\frac{\partial v}{\partial x} + u\frac{\partial^2 v}{\partial x \partial y} + \left(\frac{\partial v}{\partial y}\right)^2 + v\frac{\partial^2 v}{\partial y^2} = -\frac{1}{\rho}\frac{\partial^2 P}{\partial y^2} + \nu\frac{\partial\left(\nabla^2 v\right)}{\partial y} \quad , \tag{3.27}$$

Adding the two previous expressions, we obtain

$$\left(\frac{\partial u}{\partial x}\right)^2 + \left(\frac{\partial v}{\partial y}\right)^2 + u\left(\frac{\partial^2 u}{\partial x^2} + \frac{\partial^2 v}{\partial x \partial y}\right) + 2\frac{\partial u}{\partial y}\frac{\partial v}{\partial x} + v\left(\frac{\partial^2 v}{\partial y^2} + \frac{\partial^2 u}{\partial x \partial y}\right)$$

$$= -\frac{1}{\rho}\frac{\partial^2 P}{\partial x^2} - \frac{1}{\rho}\frac{\partial^2 P}{\partial y^2} + \nu\frac{\partial\left(\nabla^2 u\right)}{\partial x} + \nu\frac{\partial\left(\nabla^2 v\right)}{\partial y} \quad , \tag{3.28}$$

$$\left(\frac{\partial u}{\partial x}\right)^2 + \left(\frac{\partial v}{\partial y}\right)^2 + u\left(\frac{\partial^2 u}{\partial x^2} + \frac{\partial^2 v}{\partial x \partial y}\right) + 2\frac{\partial u}{\partial y}\frac{\partial v}{\partial x} + v\left(\frac{\partial^2 v}{\partial y^2} + \frac{\partial^2 u}{\partial x \partial y}\right)$$

$$= -\frac{1}{\rho}\nabla^2 P + \nu\nabla^2\left(\frac{\partial u}{\partial x} + \frac{\partial v}{\partial y}\right) \quad . \tag{3.29}$$

Replacing u and v from the stream function definition

$$\left(\frac{\partial^2\psi}{\partial x\partial y}\right)^2+\left(-\frac{\partial^2\psi}{\partial x\partial y}\right)^2+\frac{\partial\psi}{\partial y}\left(\frac{\partial^2 u}{\partial x^2}+\frac{\partial^2 v}{\partial x\partial y}\right)-2\frac{\partial^2\psi}{\partial y^2}\frac{\partial^2\psi}{\partial x^2}-\frac{\partial\psi}{\partial x}\left(\frac{\partial^2 v}{\partial y^2}+\frac{\partial^2 u}{\partial x\partial y}\right)$$

$$=-\frac{1}{\rho}\nabla^2 P+\nu\nabla^2\left(\frac{\partial u}{\partial x}+\frac{\partial v}{\partial y}\right) \quad , \tag{3.30}$$

$$2\left(\frac{\partial^2\psi}{\partial x\partial y}\right)^2+\frac{\partial\psi}{\partial y}\underbrace{\left(\frac{\partial^3\psi}{\partial x^2\partial y}-\frac{\partial^3\psi}{\partial x^2\partial y}\right)}_{0}-2\frac{\partial^2\psi}{\partial y^2}\frac{\partial^2\psi}{\partial x^2}-\frac{\partial\psi}{\partial x}\underbrace{\left(-\frac{\partial^3\psi}{\partial x\partial y^2}+\frac{\partial^3\psi}{\partial x\partial y^2}\right)}_{0}$$

$$=-\frac{1}{\rho}\nabla^2 P+\nu\nabla^2\underbrace{\left(\frac{\partial^2\psi}{\partial x\partial y}-\frac{\partial^2\psi}{\partial x\partial y}\right)}_{0} \quad , \tag{3.31}$$

$$2\left(\frac{\partial^2\psi}{\partial x\partial y}\right)^2-2\frac{\partial^2\psi}{\partial y^2}\frac{\partial^2\psi}{\partial x^2}=-\frac{1}{\rho}\nabla^2 P \quad . \tag{3.32}$$

Leading finally to:

$$\nabla^2 P=2\rho\left[\left(\frac{\partial^2\psi}{\partial x^2}\frac{\partial^2\psi}{\partial y^2}\right)-\left(\frac{\partial^2\psi}{\partial x\partial y}\right)^2\right] \quad . \tag{3.33}$$

The equations (3.13,3.25,3.33) form a system of non-linear elliptic equations equivalent to the original equations (3.3 - 3.5). This system of equations is convenient, since if we are finding just the velocities, we just need to solve the equations 3.13 and 3.25

simultaneously, without taking into account the pressure. We need to remark that the original equations (3.3 - 3.5) are coupled and to obtain the velocity we need to solve the system of three equations simultaneously, but with the change of variable, the stream function and vorticity are uncoupled from the pressure and we just need to solve two equations. If we want to calculate the pressure, this can be obtained by solving 3.33 after finding the values for ψ and ζ.

Chapter 4

INTRODUCTION TO SPECTRAL METHODS

The idea of this project is to implement an emerging technology to solve partial differential equations, which in some cases is a better alternative to the well known Finite Difference and Finite Element approach. The appeal of this new approach, called Spectral Methods, relies on the much better rate of convergence compared to that of finite differences without the use of fine grids for the discretization; while fourth order finite difference would require in many cases thousands of points to achieve certain accuracy (fourth order convergence), spectral methods could reach machine precision with grids as small as 40 points, behavior called spectral accuracy.

The idea behind this great improvement in the convergence rate is based on polynomial interpolation not over equispaced grid points (which would lead to Runge phenomenon) but over grids with a higher concentration of points near the boundaries [13]. One particular set of points where the interpolation by polynomials becomes very small is the Chebyshev collocation [14]:

$$x_j = \cos(j\pi/N) \tag{4.1}$$

This concentration can be easily visualized as the projections of the equispaced points over the unit circle on the interval $[-1, 1]$ [13] as show in the following figure:

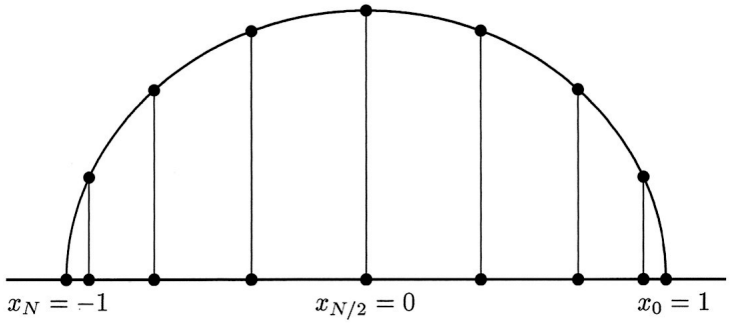

Figure 4.1: Chebyshev collocation on the interval $[-1, 1]$ (see [13])

With this approach, the resulting differentiation matrices differ with those resulting from the equispaced finite difference approach in the following way: In the case of

Finite difference, as that of the one used for our first project, the finite difference representation of the derivatives is very intuitive and approachable (hence its appeal), where the centered first derivative of second order of accuracy can be represented as $\frac{\partial \psi}{\partial x}\Big|_{i,j} = \frac{\psi_{i+1,j} - \psi_{i-1,j}}{2\Delta x} - O\left[(\Delta x)^2\right]$ [12], and to achieve higher orders of accuracy would just require larger stencils where the derivative can be approximated by an algebraic relation of the value of the function at more points. On the other hand, in spectral differentiation, the derivative of the function is approximated by taking into account each and every point where the function is known. In this sense spectral differentiation can be seen as a finite difference approximation of limiting order, where the stencil used is the whole grid. But there is a catch; if we just increase the stencil size to obtain a higher accuracy over an equispaced grid, the weights needed in the approximation of the derivatives close to the boundaries (which will not be centered approximations any more) will be very large and will generate large errors. This growth on the weights on the differentiation matrix can be avoided if we use a grid with clustered points near the boundaries, in particular, if we use Chebyshev collocation [For98]. This approach of limiting order of accuracy will generate dense differentiation matrices compared with the sparse versions of finite difference, but will allow us to reach higher accuracy with much smaller grids.

Chapter 5

DISCRETIZATION OF THE SYSTEM

The system that we are interested in, is the flow past a circular cylinder. We want to simulate how the streamlines of free flow are perturbed after placing the obstacle. We will use the symmetry of the system so that we just need to solve the equations for the upper half plane:

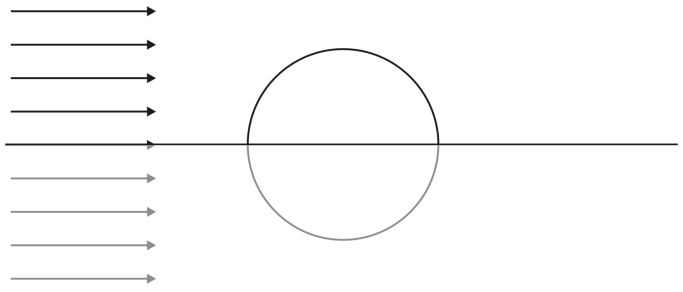

Figure 5.1: Circular Cylinder in plane flow

For this system a rectangular discretization is not the best approach. To obtain a grid that fits better the physical system, we will use the conformal mapping suggested by Fornberg[8], that maps

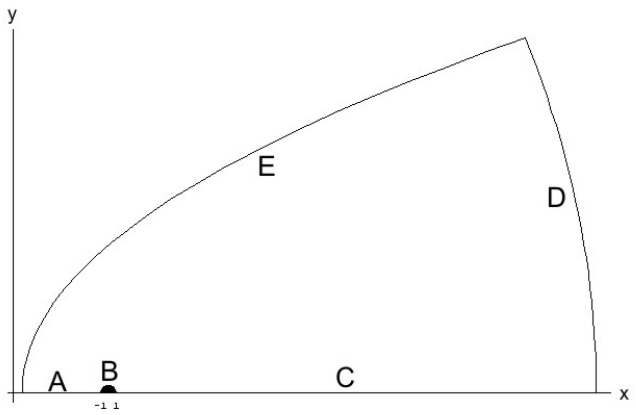

Figure 5.2: Physical Domain (X Plane)

To

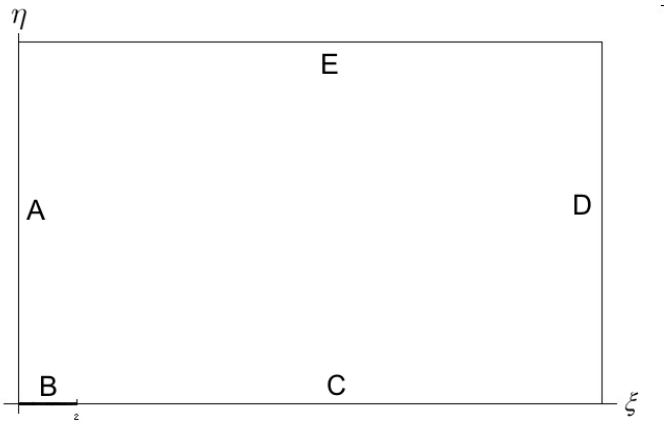

Figure 5.3: Mapped Domain (Z Plane)

via the conformal mapping

$$Z = \sqrt{X} - \frac{1}{\sqrt{X}} \tag{5.1}$$

In this new domain the equations (3.13,3.25) are transformed into

$$J\nabla^2\psi = \zeta \quad . \tag{5.2}$$

$$\nabla^2\zeta = \frac{Re}{2}\left[\frac{\partial\psi}{\partial\xi}\frac{\partial\zeta}{\partial\eta} - \frac{\partial\psi}{\partial\xi}\frac{\partial\zeta}{\partial\eta}\right] \quad . \tag{5.3}$$

where J is the Jacobian of the transformation:

$$J = \left|\frac{dZ}{dX}\right| \tag{5.4}$$

Then our plan is to solve the system of equations for a rectangular domain (*the Z Plane*):

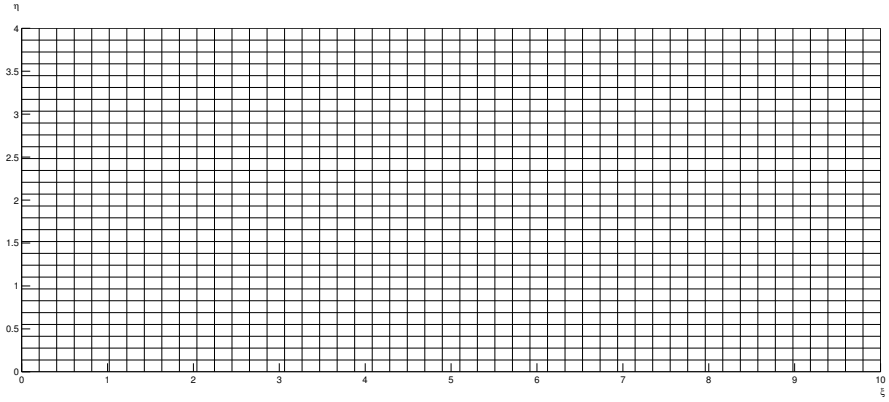

Figure 5.4: Rectangular Grid in the Z Plane

and then return the solution to the physical domain by inverting the map, that is

$$X = \frac{Z^2 - 2 \pm Z\sqrt{Z^2 - 4}}{2} \tag{5.5}$$

Mapping the rectangular grid to

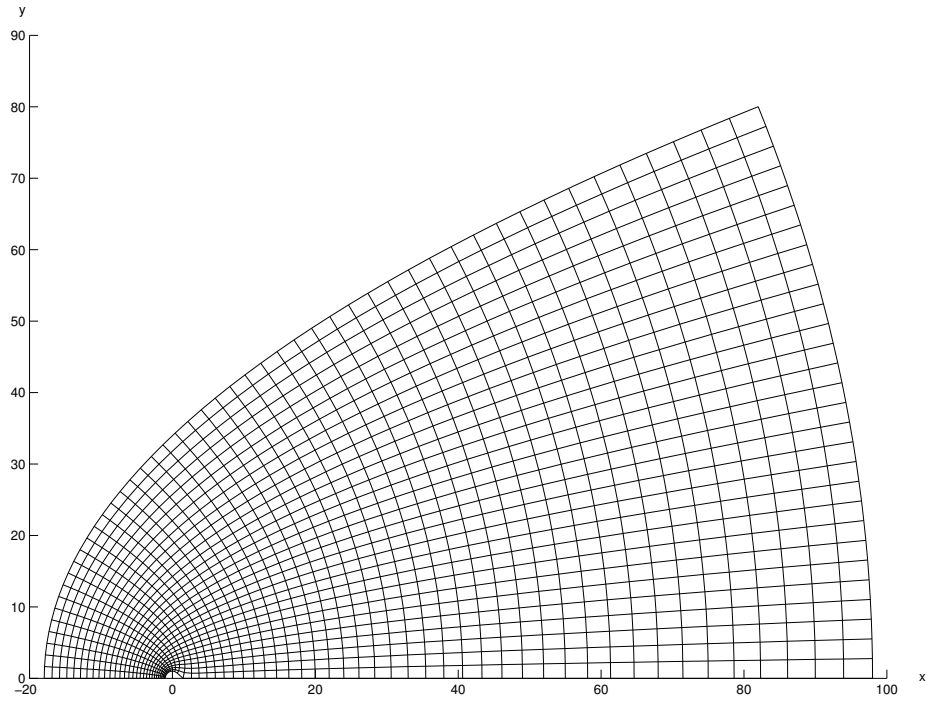

Figure 5.5: Rectangular Grid mapped back to the X Plane

In our first attempt to implement spectral methods, we used Chebyshev collocation in both directions of our domain, resulting grids as the following figure:

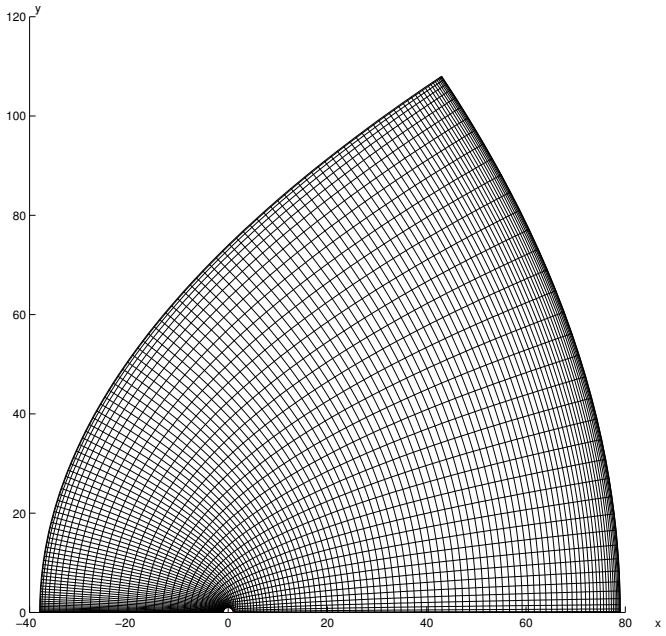

Figure 5.6: Chebyshev collocation in both ξ and η directions

This collocation proved to be inefficient due to unnecessary concentration of points in regions of the physical domain where not much is happening (low gradients) as the region of the left before interacting with the circular cylinder and the region of far flow in the far right; and was not resolved enough in regions of interest where the gradients are higher, as the obstacle and the part immediately behind the obstacle. We decided then to use a combination of spectral and finite difference methods, with Chebyshev collocation in the η direction and equispaced grid in the ξ direction as illustrated in the following figure:

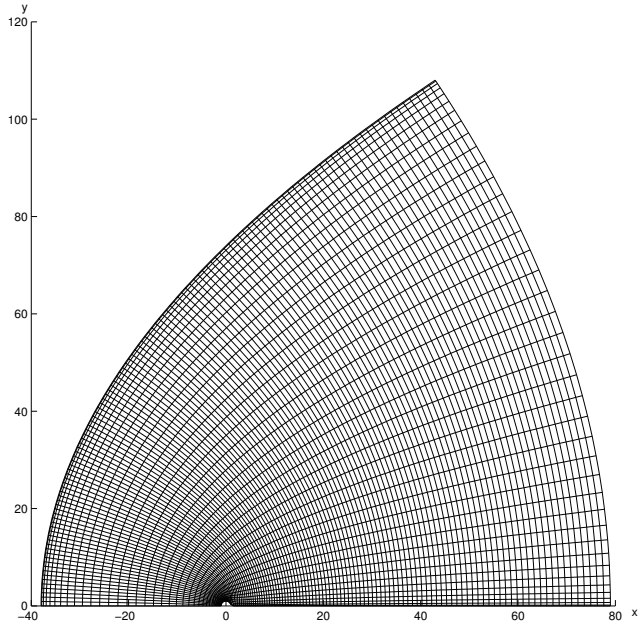

Figure 5.7: Chebyshev collocation in the η direction and equispaced collocation in the ξ direction

We still wanted to get a better resolution close to the obstacle, moving the downstream boundary farther and without wasting computer time calculating fine grids in that region. We decided to use an exponential stretching in the ξ direction that allow us to move that boundary farther away without sacrificing any resolution close to the obstacle. In this case we implemented a subroutine developed by Bengt Fornberg, in a way that we were able to do arbitrary stretchings with ease to fit the needs of resolution in the required areas. The resulting grid was the following:

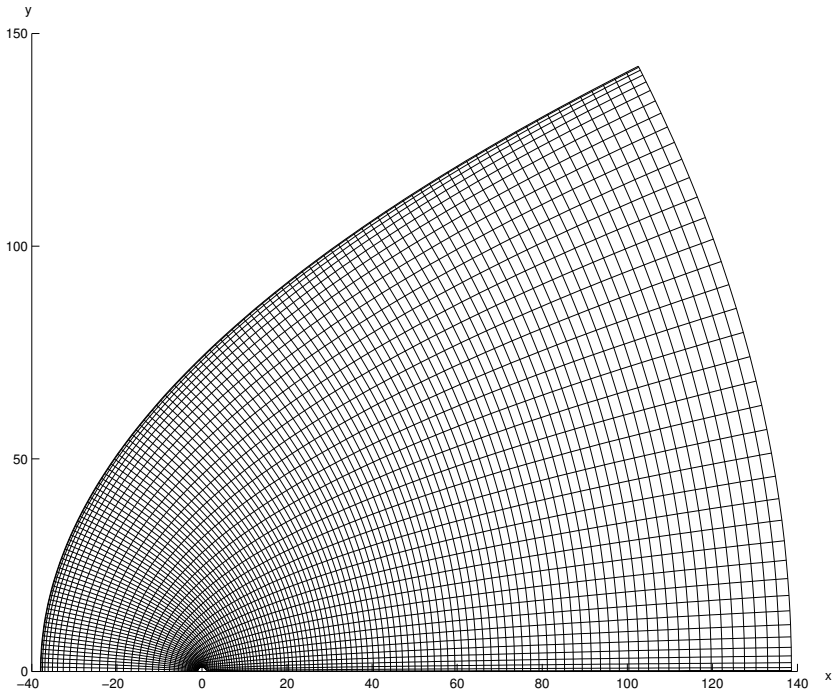

Figure 5.8: Chebyshev collocation in the η direction and exponential collocation in the ξ direction

Chapter 6

SOLUTION SCHEME

The non-linear nature of the Navier-Stokes equations makes the solution process very challenging. In our previous work we used an iterative scheme based on Gauss-Seidel/Successive Over-Relaxation Methods (SOR). Now we will use Newton's as in [9] but implementing spectral differentiation.

Newton's method (or Newton Raphson method) is a well known method for finding successive approximations to zeros of a function, which is very powerful given that it converges in a few iterations (quadratic convergence) provided that we have a good initial guess. Given a function $f(x)$ and its derivative $f'(x)$, starting with a guess x_{old} we can obtain a better approximation to the zero of the function simply by computing $x_{new} = x_{old} - \frac{f(x_{old})}{f'(x_{old})}$. In the case of solving a nonlinear system of partial differential

equations like the problem at hand, we replace the division by $f'(x)$ and instead we multiply on the left by the inverse of the Jacobian H^{-1} of the operator representing the system; each iteration then becomes

$$X_{new} = X_{old} - H^{-1}F(X_{old}), \tag{6.1}$$

where the inverse is not actually calculated but instead the process is replaced by solving the system of linear equations

$$H(X_{old})(X_{new} - X_{old}) = -F(X_{old}). \tag{6.2}$$

The matrix representation of theses operators can be studied as follows: recall the system of equations under study 3.13 and 3.25 and let us represent the partial derivatives by subindices, the laplacian operator ∇^2 by Δ and the negative of the vorticity ζ by w. Simplifying our notation we then write the set of equations as:

$$\Delta\psi + w = 0 \quad , \tag{6.3}$$

$$\Delta w + \frac{Re}{2}\left[\psi_y w_x - \psi_x w_y\right] = 0 \quad . \tag{6.4}$$

We let X be the $2MN \times 1$ matrix containing both the values of stream and vorticity as follows

$$X = \left[\begin{array}{c} \psi \\ \hline \omega \end{array}\right] \quad , \tag{6.5}$$

then the system can be written as $F(X) = 0$ where the operator F can be written as

$$F(X) = L(X) + NL = 0 \quad , \tag{6.6}$$

with L and NL being the linear and non-linear parts of the operator:

$$L = \left[\begin{array}{c|c} Lap & I \\ \hline 0 & Lap \end{array}\right], \qquad NL = \frac{Re}{2}\left[\begin{array}{c} 0 \\ \hline D_y\psi D_x\omega - D_x\psi D_y\omega \end{array}\right]. \tag{6.7}$$

Then

$$F\left[\begin{array}{c}\psi\\ \hline \omega\end{array}\right]=\left[\begin{array}{c|c}Lap & I\\ \hline 0 & Lap\end{array}\right]\left[\begin{array}{c}\psi\\ \hline \omega\end{array}\right]+\frac{Re}{2}\left[\begin{array}{c}0\\ \hline D_y\psi D_x\omega - D_x\psi D_y\omega\end{array}\right]=0. \tag{6.8}$$

Now to obtain the Jacobian matrix H (linearization) of the operator F we start by analyzing the following perturbations, let Ψ and Ω be the stream and vorticity functions and let ψ and ω be its corresponding perturbations: $\Psi \rightarrow \Psi + \psi$ and $\Omega \rightarrow \Omega + \omega$.

Let us look now at the propagation of the perturbations in the Navier-Stokes equations

$$\Delta(\Psi+\psi)+(\Omega+\omega)=0 \quad , \tag{6.9}$$

$$\Delta(\Omega+\omega)+\frac{Re}{2}\Big[(\Psi+\psi)_y(\Omega+\omega)_x-(\Psi+\psi)_x(\Omega+\omega)_y\Big]=0 \quad . \tag{6.10}$$

Then the second equation is

$$\Delta(\Omega+\omega)+\frac{Re}{2}\Big[(\Psi_y+\psi_y)(\Omega_x+\omega_x)-(\Psi_x+\psi_x)(\Omega_y+\omega_y)\Big]=0 \quad ,$$

$$\Delta(\Omega+\omega)+\frac{Re}{2}\Big[(\Psi_y\Omega_x+\Psi_y\omega_x+\psi_y\Omega_x+\psi_y\omega_x)-(\Psi_x\Omega_y+\Psi_x\omega_y+\psi_x\Omega_y+\psi_x\omega_y)\Big]=0 \quad .$$

Discarding second order terms and regrouping

$$\Delta\Omega+\frac{Re}{2}\Big[\Psi_y\Omega_x-\Psi_x\Omega_y\Big]+\Delta\omega+\frac{Re}{2}\Big[(\Psi_y\omega_x+\psi_y\Omega_x)-(\Psi_x\omega_y+\psi_x\Omega_y)\Big]=0 \quad . \tag{6.11}$$

Obtaining

$$\{\Delta\Psi+\Omega\}+\{\Delta\psi+\omega\}=0 \quad , \tag{6.12}$$

$$\left\{\Delta\Omega+\frac{Re}{2}\Big[\Psi_y\Omega_x-\Psi_x\Omega_y\Big]\right\}+\left\{\Delta\omega+\frac{Re}{2}\Big[(\Psi_y\omega_x+\psi_y\Omega_x)-(\Psi_x\omega_y+\psi_x\Omega_y)\Big]\right\}=0 \quad . \tag{6.13}$$

Then the Jacobian matrix (linearization) of the operator is

$$H = \left[\begin{array}{c|c} Lap & I \\ \hline 0 & Lap \end{array}\right] + \frac{Re}{2}\left[\begin{array}{c|c} 0 & 0 \\ \hline D_x\omega D_y - D_y\omega D_x & D_y\psi D_x - D_x\psi D_y \end{array}\right] . \tag{6.14}$$

Chapter 7

BOUNDARY CONDITIONS

As we noted previously, the equations governing the fluid flow are elliptic, so that we have an equilibrium problem expressed as a *Boundary Value Problem*. In this way, the boundary conditions determine the solution in the complete domain. The vorticity and the region where all the interesting phenomena take place is inside the physical domain (Figure 5.2), and we can assume that outside this region the vorticity is zero and the incoming plane flow enters unperturbed into the domain.

The boundary condition need to be carefully set to represent correctly the physics of the problem. Refering again to figure 5.2, the boundary conditions on A and C are determined by symmetry. On B the normal velocities on the obstacle are also zero. In this way the line ABC is a stream line and we can impose $\psi = 0$ given that the

physical meaning of ψ depends only in its derivatives and not any additive constant (*as shown in 3.6*). We then have the following Dirichlet condition:

$$\psi = 0 \quad \text{in} \quad \mathbf{A, B, C} \tag{7.1}$$

Using the same symmetry argument, the vorticity in A and C must be zero:

$$\zeta = 0 \quad \text{in} \quad \mathbf{A, C} \tag{7.2}$$

We can choose **D** far enough from the obstacle to consider a free flow condition. Then we have the following Neumann condition:

$$\frac{\partial \psi}{\partial x} = 0 \quad . \tag{7.3}$$

To express this condition in our mapped domain we can write

$$\frac{\partial \psi}{\partial \xi} = \underbrace{\frac{\partial \psi}{\partial x}}_{0} \frac{\partial x}{\partial \xi} + \underbrace{\frac{\partial \psi}{\partial y}}_{V_0=1} \frac{\partial y}{\partial \xi} \tag{7.4}$$

Then

$$\frac{\partial \psi}{\partial \xi} = \frac{\partial y}{\partial \xi} \quad \text{in} \quad \mathbf{D} \tag{7.5}$$

Similarly

$$\frac{\partial \zeta}{\partial \xi} = \frac{\partial y}{\partial \xi} \quad \text{in} \quad \mathbf{D} \tag{7.6}$$

Expressing that the vorticity does not change beyond the end of the domain.

And for E sufficiently far from the obstacle we can say that the vorticity is negligible and the incoming flow enters the domain freely as potential flow:

$$\psi = \psi_{pot} \quad \text{in} \quad \mathbf{E} \tag{7.7}$$

and

$$\zeta = 0 \quad \text{in} \quad \mathbf{E} \tag{7.8}$$

However, for our specific conformal map, as the Reynolds number increases we will see that the perturbation generated by the obstacle starts getting closer to **E** and while the vorticity remains close to zero, the flow cannot be aproximated by potential flow. We then calculate this boundary condition as in [9] by placing an array of point vortices close to the boundary and observing how the top row of points can be calculated from the row of points right before the boundary in a way that we do not pick any exponentially growing modes[9]:

$$\begin{bmatrix} \\ \psi_{top} \\ \\ \end{bmatrix} = A \begin{bmatrix} \\ \psi_{top-1} \\ \\ \end{bmatrix} \tag{7.9}$$

In this way, we can use this behavior as a non-local boundary condition by solving for the matrix A and using it to calculate the top row from the previous row in general.

7.1 Second Boundary condition on the Obstacle

We already have one of the boundary conditions on the obstacle which is $\psi = 0$. However, the second boundary condition is also a condition on the stream function called the No-slip Boundary condition, which states that there is no tangential velocity on the obstacle:

$$\frac{\partial \psi}{\partial \eta} = 0 \tag{7.10}$$

The lack of a condition for the vorticity in the obstacle has been considered by some authors to lead to a degenerate system of equations, and was avoided in our previous work by using finite differences to express this condition as a condition for the vorticity[12], an approximation that would have destroyed the spectral accuracy in our new approach. Analyzing this problem carefully we can see that the two conditions on the stream function are enough to solve the system of equations if the system is treated as a whole. That is, we can no longer solve one equation for the stream function and then one equation for vorticity as we did with SOR methods.

The implementation of the boundary conditions in the case of Finite Differences with SOR methods was very intuitive and straightforward, since at every iteration we just needed to relax interior points in the domain and recalculate Neumann boundary conditions on certain boundaries, while leaving fixed values of the Dirichlet boundary conditions unchanged. Now, we need to have one big system of equations that not only includes the equations to be solved in the interior points, but also all the imposed boundary conditions. Hence, the difficulty of the approach.

We include then all the boundary conditions on our operators on every Newton's iterative step (6.1), keeping in mind that each row of the Jacobian will be an equation, and each column will be an unknown, and that the system must include as many equations as unknowns. Therefore, if the discretization of the system includes $M \times N$ points, the system must have $2MN$ equations (Stream and vorticity), from which $(M-2)(N-2)$ equations will be equations to be solved in the interior points and the rest should be boundary conditions to be satisfied. In this way, we can represent the full Jacobian as:

$$H = \left[\begin{array}{c|c} H_i & \text{Interior} \\ \hline I & \text{Dirichlet} \\ \hline A_{top-1} - I_{top} & \text{Non} - \text{local} \\ \hline D_y & \text{Neumann} \end{array}\right], \tag{7.11}$$

Where H_i is the part of the Jacobian corresponding to the interior points, as given by (6.14). After replacing some of the rows by the equations corresponding to the boundary conditions, we need to make the corresponding change in the right-hand side of the equation to be in accordance to these conditions, that is we need to construct the right hand side of the equation (6.2) as follows:

$$RHS = \left[\begin{array}{c|c} -F(X_{old}) & \text{Interior} \\ \hline 0 & \text{Dirichlet} \\ \hline 0 & \text{Non} - \text{local} \\ \hline 0 & \text{Neumann} \end{array}\right]. \tag{7.12}$$

Note that by having the Identity on the Dirichlet rows of H we are assuring that

on each correction step of the Newton's Method, the change on the boundary points specified by I is 0, that is, our initial guess should of course satisfy the boundary conditions. On the non-local boundary section the equation to be satisfied is (7.9) in the form $A\psi_{top-1} - I\psi_{top} = 0$. Similarly to the Dirichlet condition, for the Neumann boundary conditions the correction at each Newton's step should have a derivative normal to the obstacle equal to zero. Therefore, we want to use an initial guess that also satisfies this boundary condition.

Chapter 8

STRUCTURE OF THE OPERATORS

In this chapter we will carefully study the structure of the operators from the discretization point of view. We studied the general structure of the operators in chapter 6 and how to include the boundary conditions in these operators. Now we want to explore the internal shape of the differentiation matrices for our combination of spectral and finite difference methods.

For the purpose of demonstration and comparison, we will show the structures of the differentiation matrices for a 40×40 discretization (instead of the finer grids used for the computations) since the important features of the boundaries and the

stencils would be hard to visualize otherwise. First, in the ξ direction, we used a 6^{th} order approximation of the derivative, resulting in a 7 point stencil. Leading to the following structure for the differentiation matrix:

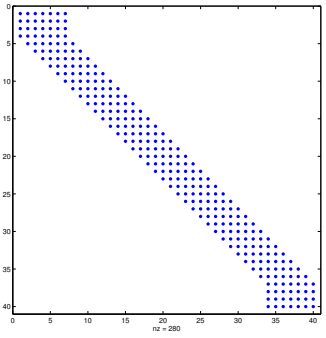

Figure 8.1: 40×40 Differentiation matrix D_ξ

On the other hand, the use of spectral methods in the η direction result in full matrices; recall that spectral method can be considered as the limiting order of finite differences, where the stencil includes every point:

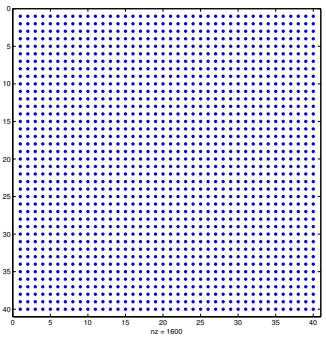

Figure 8.2: 40×40 Differentiation matrix D_η

Note that this differentiation matrices can be used to calculate the derivative in the ξ or η direction when multiplied by a column vector containing the elements of a row or column of our matrix containing the values of the stream or vorticity. However, we want to be able to differentiate the whole matrix of stream or vorticity with respect to ξ and η, when this matrix is represented as one single vector as proposed in the chapter of the solution scheme. This first differentiation operator was not only used in the second of the Navier-Stokes equations, but specific rows were also used in the Neumann boundary conditions as explained in previous chapters. In this way, the full differentiation matrix with respect to $\xi$and η can be calculated by using the tensor product (or Kronecker product) $D_{\xi-\text{full}} = D_\xi \otimes I_\eta$ and $D_{\eta-\text{full}} = I_\xi \otimes D_\eta$ where I_η and I_ξ are the identity matrices of the sizes corresponding to each diection. These products result in the following structures:

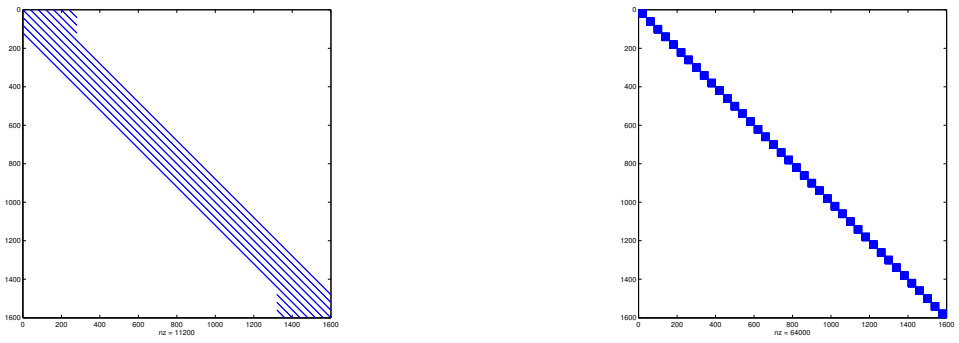

Figure 8.3: Structure of the operators $D_{\xi-\text{full}} = D_\xi \otimes I_\eta$ and $D_{\eta-\text{full}} = I_\xi \otimes D_\eta$

In a similar way the Laplacian operator is then calculated as $L = I_\xi \otimes D_\eta^2 + D_\xi^2 \otimes I_\eta$ with structure:

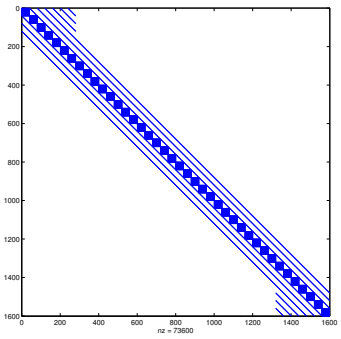

Figure 8.4: Structure of the Laplacian

Now, recall the structure of the Jacobian from 6.14 which including the boundary conditions is then

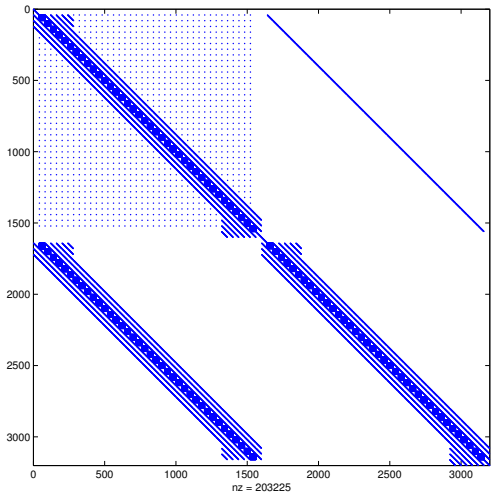

Figure 8.5: Structure of the Jacobian

We can see how the structure resembles that shown in 6.14, while the some of the Dirichlet boundary conditions can be seen as identity elements in the top left corner, center and bottom right corner of the Jacobian. The grid of points in the upper left section of the matrix corresponds to the nonlocal boundary conditions.

Chapter 9

COMPUTATIONS

In this chapter we will discuss the computations and the program used to solve the system of equations. The details shown in this chapter are sometimes overlooked in this type of project, but they are as fundamental as the theoretical counterpart, and we will strive to show the beauty of some of the elements that were key to achieving the results shown in the following chapters.

Compared to our previous work in 2004 [12] (FORTRAN90 was used together with the graphical subroutines PGPLOT), we decided to use MATLAB because its tremendous accessibility and power to handle sparse matrices, availability of sparse solvers and many other tools. MATLAB also allows easy implementation of programs that will take full advantage of 64-bit processor architecture together with 64-bit

operating systems, and hence, is able to handle larger memory addresses, essential for our demands.

However, even with all these tools available in MATLAB, a successful implementation of this combination of spectral and finite difference methods for a non-linear system of equations like the Navier-Stokes Equations is not a simple task, and we will guide you through the general structure of the program and some of the key ideas that made this implementation possible.

First, our system was discretized as shown in (Chap. 5), with only 40 points in the η direction, this small number of discretization points is possible due to its careful collocation and the use of spectral methods in this direction (Chap. 4); 160 points were used in the ξ direction where 6th order Finite Difference was implemented. (Different discretizations were also tested to check for grid dependence of the results).

After defining the parameters used to generate the grid, we created a program to make the collocation of the points depending on specified options that gave us the ability to easily compare the results of using spectral methods in both directions or to switch equispaced or different types of stretching in the ξ direction.

The differentiation matrices were then created by the use of another subroutine which internally calls a subroutine developed by B. Fornberg [14]. This implementa-

tion was so versatile, that choosing different parameters in the creation of the grid was enough to generate the matching differentiation matrix for the given grid.

At this point, one more subroutine was used to create a matrix with the information on the type of boundary conditions that should be used at every boundary. The importance of this matrix resides in the fact that the program will later refer to this matrix in order to decide which rows to replace in the structure of the Jacobian with the equation of the corresponding boundary condition (7.11). With this robust implementation of the boundary conditions we were able to use the same program even for a different geometry with a different placing of the boundary conditions as the one explored in Chapter 12.

We are ready now to start Newtons method: first we load a good initial guess that satisfies all boundary conditions. This initial guess was obtained first by solving the system with 0 vorticity to get the solution for Reynolds number 1 and then solutions at previous Re were used as initial guess to calculate the solution at higher Re.

At every step of the Newtons method (see 6.2) the system of equations was solved using the subroutine cholsol (sparse Cholesky factorization) from the package CXSparse, which is the 64-bit version of the package CSparse developed by Tim Davis [15]. This subroutine can be found on MATLAB Central and some of its subroutines will be part of future releases of MATLAB. The Sparse Backslash operator included

in MATLAB would give the same results, but the use of the 64-bit version of the subroutines showed improvement in computation time.

Only 4 to 5 iterations were necessary to obtain convergence $O(\text{correction}) = 10^{-12}$, and at that point the result was used as an initial guess for a higher Reynolds number. Note that one single step of 6.2 required the use of three different subroutines, one to calculate F at the previous step with the corresponding elements of the boundary conditions replaced, one to calculate the Jacobian that includes the boundary conditions and one to solve the sparse system.

Finally solutions were saved as the program was converging for increasing Reynolds numbers, and one last subroutine was used to graph the results back in the physical domain.

Chapter 10

Stream Function and Vorticity

As explained in Chapter 9, the initial guess was obtained first by solving the system with 0 vorticity to get the solution for Reynolds number 1. The initial guess can be visualized by the following stream function:

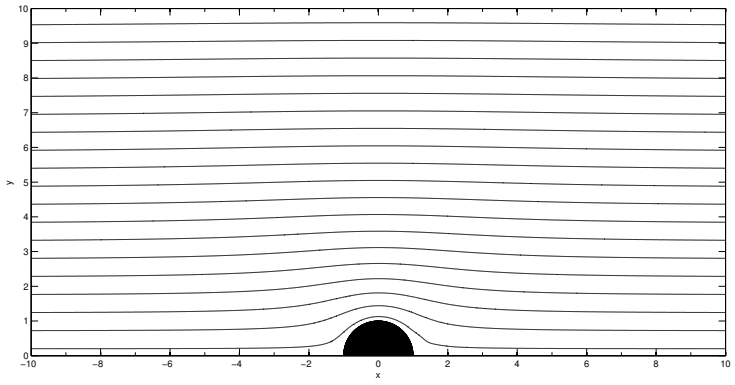

Figure 10.1: Stream Function for Potential Flow

With this solution, we started increasing the Reynolds number by steps of 10 and we were able to converge to solutions up to Re=550 where the process becomes unstable and the limitations in memory did not allow us to consider finer grids than the ones implemented. The appendix A shows a table with densities and viscosities for some fluids. In this way, we can relate the results shown with systems of practical interest, but we have to be careful since as we noted previously in reality the physical instabilities will destroy the wake bubble. We need to remark that the Reynolds number totally characterizes the fluid in terms of stream function, zones of vorticity, detachment of the boundary layer and properties of the wake bubble. Moreover, since it includes the density of the fluid ρ, its dynamic viscosity μ, the incident velocity U_∞, and the size of the obstacle L, the same Reynolds number can characterize an infinite number of cases of interest. For example by doubling the Reynolds number, we can be characterizing the same fluid at double velocity, or the same fluid perturbed by an obstacle of double size, or fluids with different density and viscosity flowing at the same velocity past the same obstacle. In this way each Reynolds number gives several possibilities.

Before we start increasing the Reynolds number, let us observe the behavior of the fluid if we have a very small Reynolds number. For $Re = 0.001$ the solution represents a flow with very high viscosity or a flow with very low speed. In both

cases the no-slip boundary condition in the obstacle keeps the flow almost still next to the obstacle and the boundary layer is a thick *coating* around the obstacle, while the stream lines have to go a longway around the obstacle

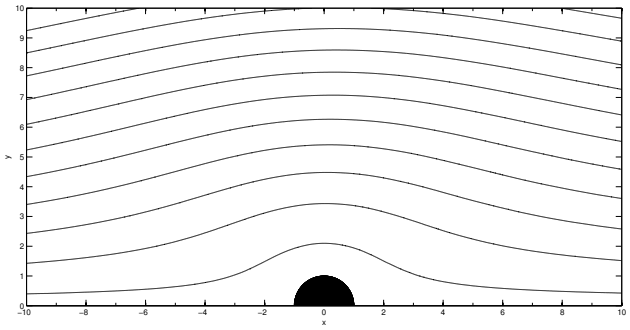

Figure 10.2: Stream Function for Re=0.001

Which would lead to the following distribution of the vorticity field:

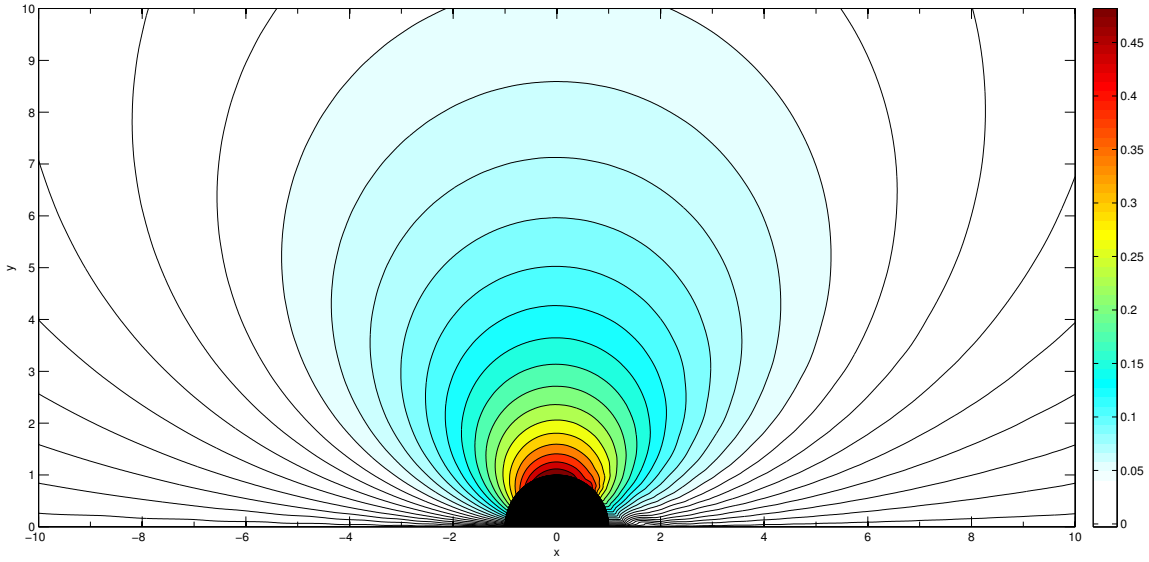

Figure 10.3: Vorticity for Re=0.001

Now, as we start increasing the Reynolds number, the flow starts showing detachment from the obstacle:

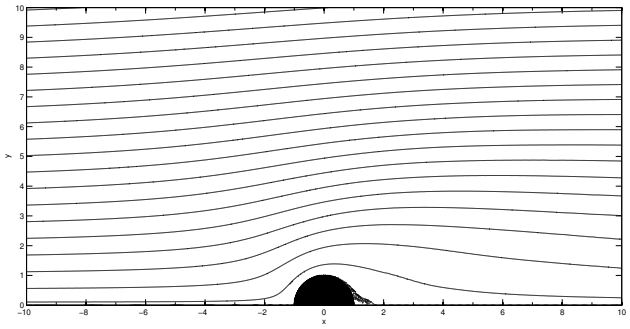

Figure 10.4: Stream Function for Re=10

And for Reynolds number 15 we can clearly see the separation of the fluid and the zone where the stream lines are closed paths and the fluid is confined behind the obstacle.

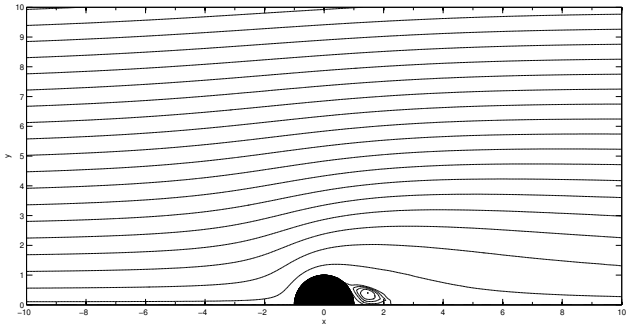

Figure 10.5: Stream Function (Closed Paths) for Re=15

With corresponding vorticity field

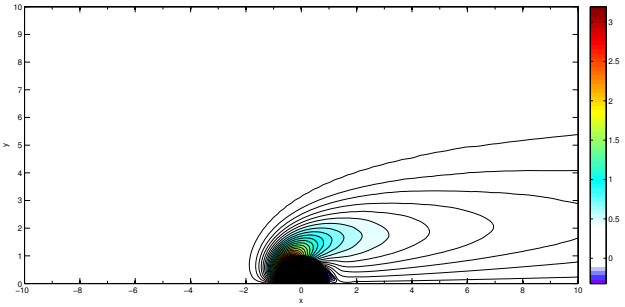

Figure 10.6: Vorticity for Re=15

Making a zoom in the obstacle we can better observe the zones where the vorticity is generated and we can clearly see the importance of having a grid with enough resolution close to the obstacle where the large gradients occur.

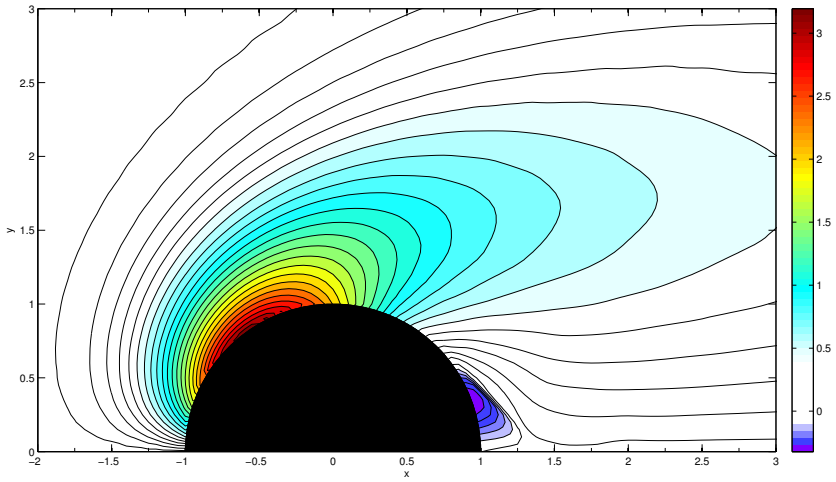

Figure 10.7: Close zoom to the obstacle. Vorticity for Re=15

We will use these results to calculate the drag force exerted by the fluid on the obstacle in section 11.

Stream Function

Figures 10.8 to 10.11 show the stream lines (level curves of the stream function) and vorticity regions for Reynolds numbers from 50 to 500; from these results we discuss features of the flow and will study how the length and width of the wake vary with Reynolds number.

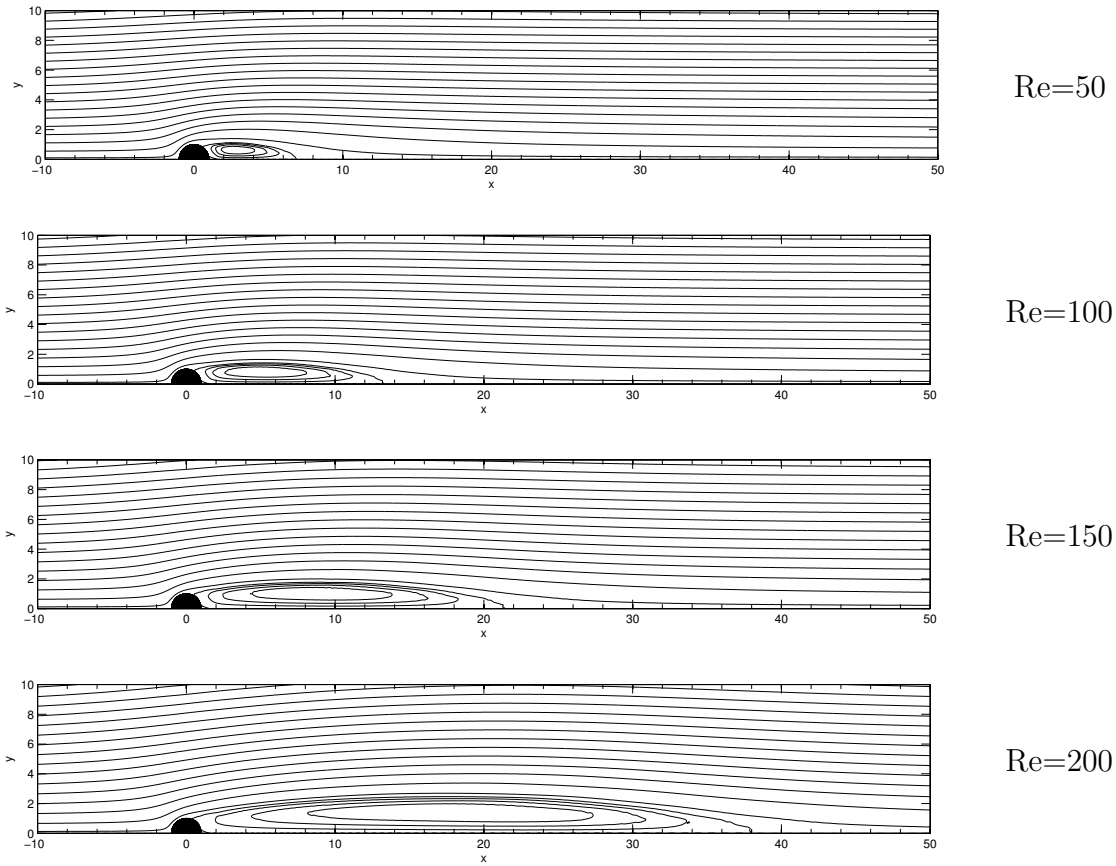

Figure 10.8: Stream Function for Re=50 to Re=200

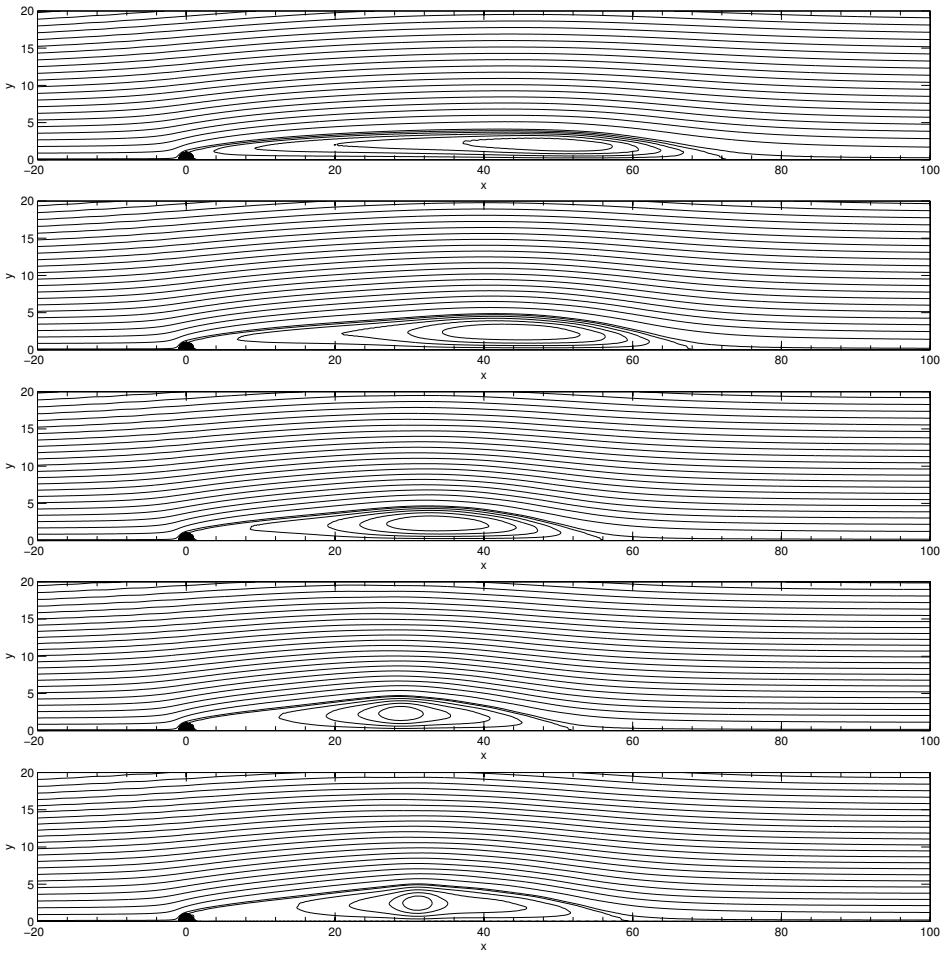

Figure 10.9: Stream Function for Re=250 to Re=500

Vorticity

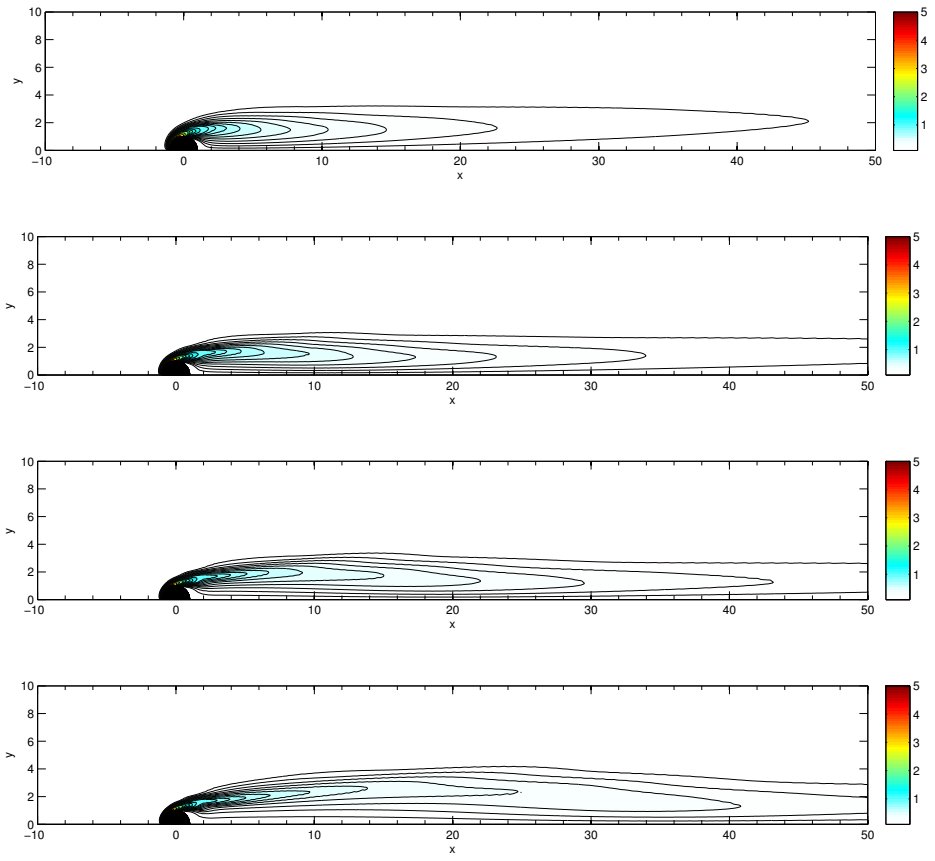

Figure 10.10: Vorticity Function for Re=50 to Re=200. Contour levels shown: 0.1, 0.2, 0.3, 0.4, 0.5, 0.6, 0.7, 0.8, 0.9, 1, 1.2, 1.4, 1.6, 1.8, 2, 2.5, 3, 4, 5.

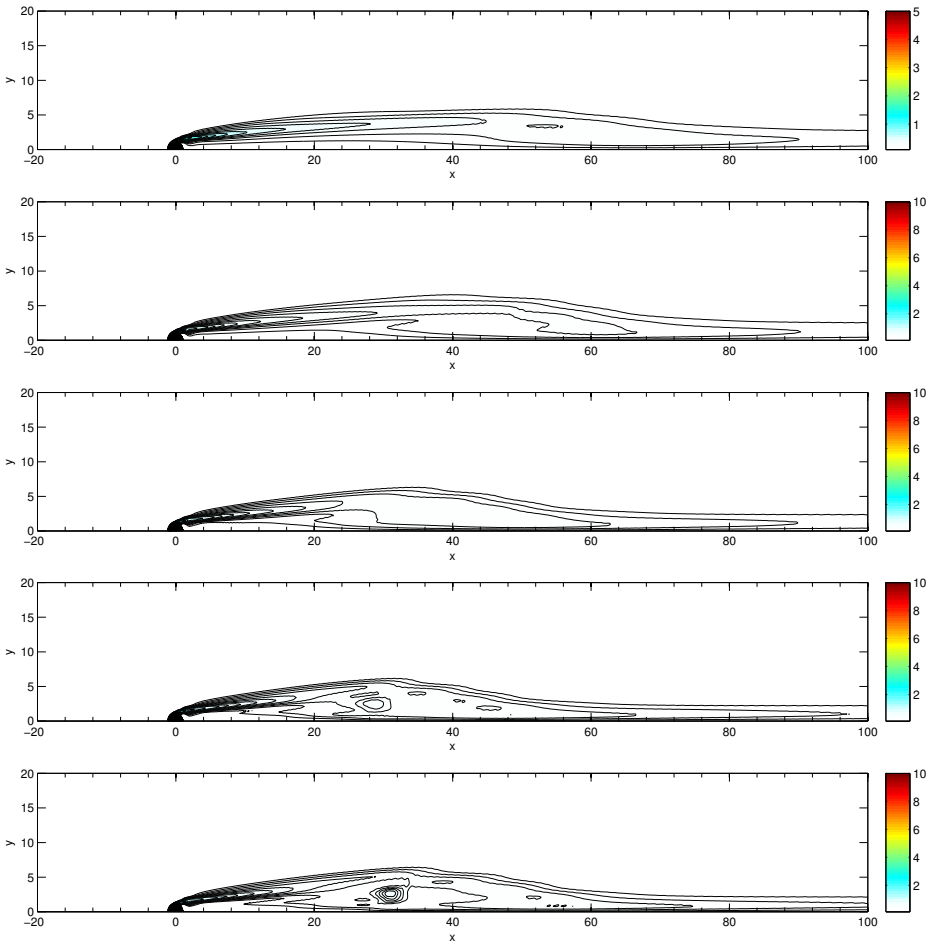

Figure 10.11: Vorticity Function for Re=250 to Re=500. Contour levels shown: 0.1, 0.2, 0.3, 0.4, 0.5, 0.6, 0.7, 0.8, 0.9, 1, 1.2, 1.4, 1.6, 1.8, 2, 2.5, 3, 4, 5.

The solutions shown were tested for grid dependency by changing the resolution of the grids. They were also tested by using different orders of the approximation as Finite difference representation of the differential operators in the ξ direction.

In these tests, characteristics of the solution like the length and width of the wake were compared and the differences were smaller than the error of the interpolation method used to measure the corresponding length or width. However, the solutions for Reynolds number close to 500 were only obtained in the finest grid. The fact that the method was reaching its limits at these values of Re do not allow us to be very confident of the results, but the method proved to be accurate for lower Reynolds numbers, leaving us with just memory capacity constraints to handle these increasingly unstable solutions. The following figures summarize the characteristics of the wake bubble.

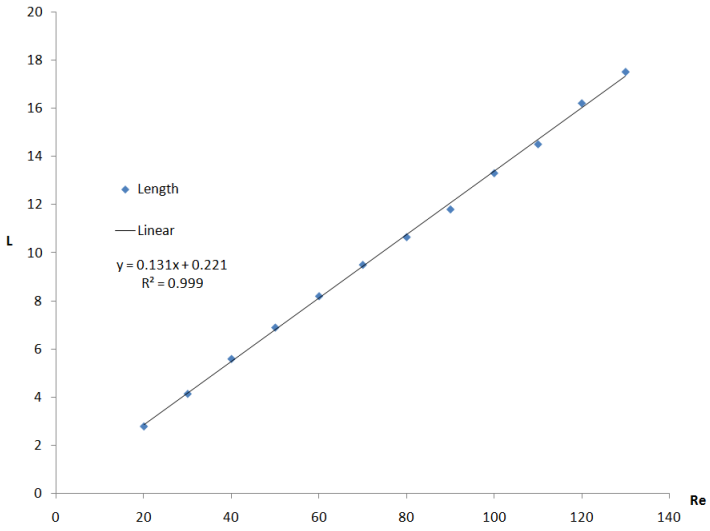

Figure 10.12: Length of the wake vs. Reynolds number for R=20 to Re=130

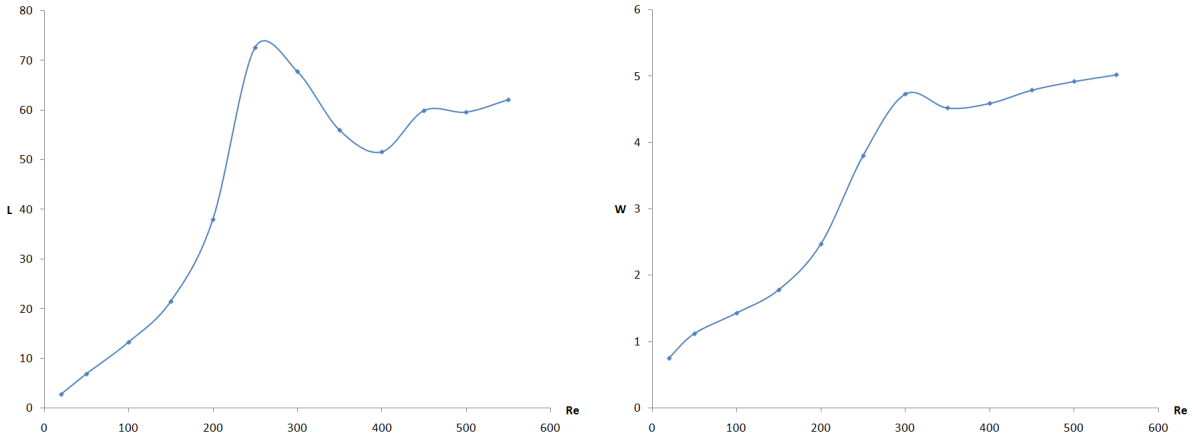

Figure 10.13: Length and width of the wake vs. Reynolds number for R=20 to Re=550

As we can see, for low Reynolds numbers, the length of the wake bubble increases linearly as the Reynolds number increases, with a coefficient of 0.131 in the linear regression. The asymptotic behavior has been shown to be linear, then the loss of linearity past Re=130 raise questions about how well resolved the system is for higher Reynolds numbers. As we mentioned before the system at higher Reynolds numbers becomes increasingly unstable and the limitations of the method in terms of computer power makes it extremely difficult to keep refining the grids.

Chapter 11

Drag Coefficient

Our study of flow past a circular cylinder is equivalent to considering a circular cylinder moving in a fluid that is still; in both cases the obstacle will experience a force exerted by the fluid, in the direction of the velocity of the fluid, or equivalently against the direction of movement of the obstacle. This force is called *Drag* and is given by

$$F_D = \frac{1}{2}\rho V^2 A C_D \quad , \tag{11.1}$$

where ρ is the density of the fluid, V is the velocity of the fluid, A is the frontal area of the obstacle and C_D is a non-dimensional coefficient that depends on the geometry of the obstacle and the Reynolds number. This coefficient has two contributions, one

due to the viscous forces and one due to the pressure on the obstacle[10]:

$$C_D = C_V + C_P, \tag{11.2}$$

where in polar coordinates

$$C_V = -\frac{8}{Re}\int_0^{\pi} \omega_{r=1} \sin\theta d\theta \tag{11.3}$$

and

$$C_P = \frac{4}{Re}\int_0^{\pi} \left[\left(\omega + \frac{\partial\omega}{\partial r}\right)_{r=1} \sin\theta\right] d\theta \tag{11.4}$$

Then

$$C_D = \frac{4}{Re}\int_0^{\pi} \left(\frac{\partial\omega}{\partial r} - \omega\right)_{r=1} \sin\theta \ d\theta \quad . \tag{11.5}$$

The integral is calculated along the surface of the obstacle and the derivative with respect to r will be calculated using spectral differentiation in the η direction:

$$C_D = \frac{4}{Re}\int_0^{\pi} \left(D_\eta\omega - \omega\right) \sin\theta \ d\theta \quad . \tag{11.6}$$

The following figures show the vorticity on the surface of the obstacle, measured in degrees from the stagnation point for different Reynolds numbers, and from these values, the corresponding calculated Drag coefficients.

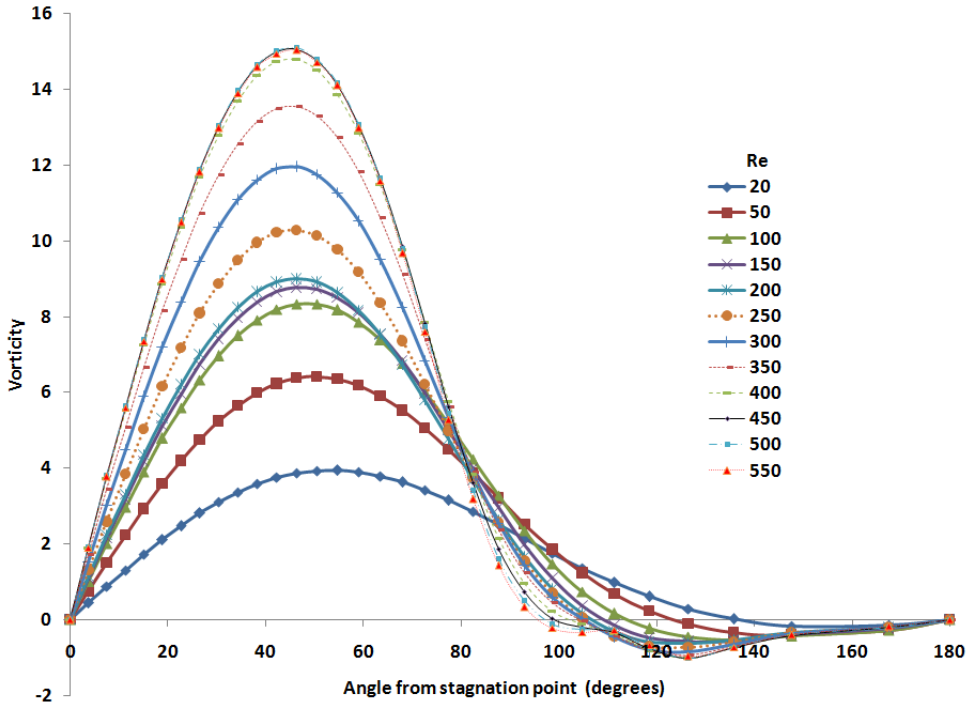

Figure 11.1: Vorticity value on the surface of the obstacle vs degrees from stagnation point

The maximum of vorticity occurs at 50 degrees from the stagnation point for the case of Re=50 but it quickly moves to 46 degrees where it stays stable from Re=100 up to Re=550. As the Reynolds number increases this maximum vorticity in the surface of the cylinder increases reaching a value of 15 at Re=450 where it seems to stabilize.

Using this values we calculated the corresponding drag coefficients. The following table presents a comparison with previous results by Fornberg[8] and Gushchin & Schennikov[19]

Re	**Vargas**	**Fornberg**	**G. & S.**
50	1.2002	—	1.519
100	1.1054	1.06	—
200	0.7884	0.833	1.167
300	0.889	0.729	0.968
400	0.9446	0.645	—
500	0.8247	0.528	0.902

Again our method was reaching its limits at Re=550, but the values of the vorticity on the surface of the obstacle coincide closely to those found by Fornberg in [8](Fig. 12) using Finite differences with larger matrices.

Chapter 12

JOUKOWSKI TRANSFORMATION

Having a robust implementation of the methods described, allow us to expand our scope to more general geometries. We decided to use another map that would allows us some versatility, the *Joukouski transormation*. This conformal map is given in its most simple form by:

$$Z = X + \frac{1}{X} \quad , \tag{12.1}$$

where as in Chapter 5 the X plane is the physical domain and the Z plane is the mapped domain where the equations will be solved *(compare with the map 5.1)*. Then via this map we will transform the upper half of the plane outside of the unit circle

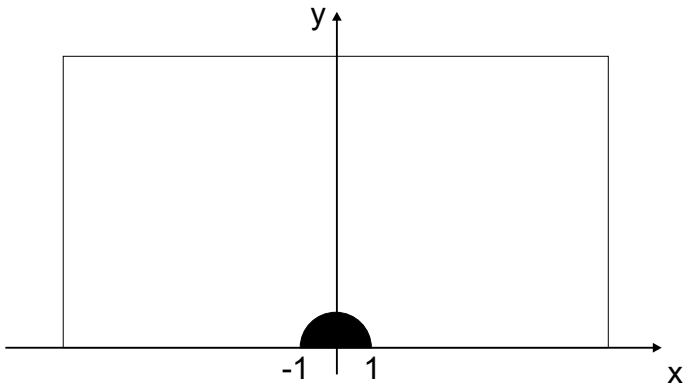

Figure 12.1: Physical Domain (X Plane)

to the upper half of the plane where the unit circle will be mapped to the strip from -2 to 2 in the x axis:

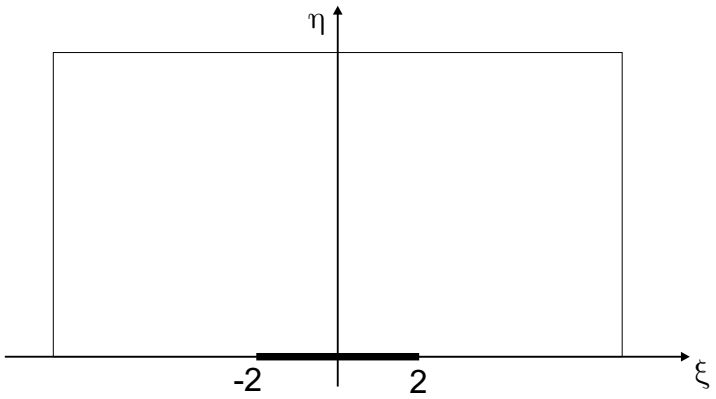

Figure 12.2: Mapped Domain (Z Plane)

Then we can solve the equations in the mapped rectangular domain similar to that of Fig. 5.4. After including some stretching to have better resolution in the regions of interest, the resulting grid becomes:

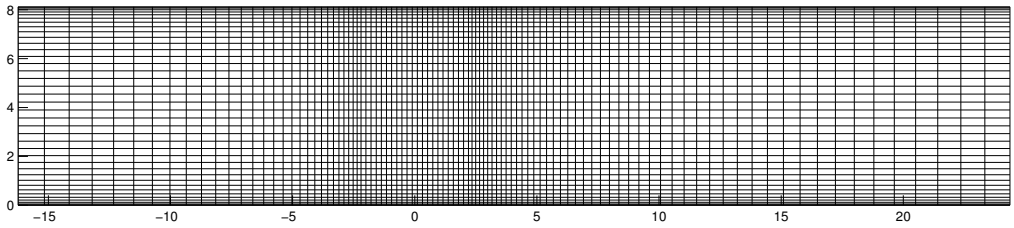

Figure 12.3: Rectangular grid in the Z Plane

Note that the grid includes an exponential stretching for the region before -2 then an equispaced grid in the section from -2 to 2 which corresponds to the obstacle and then another exponential stretching after 2. With this carefully designed grid collocation we can solve the system of equations and then return the solution to the physical domain by inverting the map:

$$X = \frac{Z \pm \sqrt{Z^2 - 4}}{2} \tag{12.2}$$

Mapping the rectangular stretched grid to

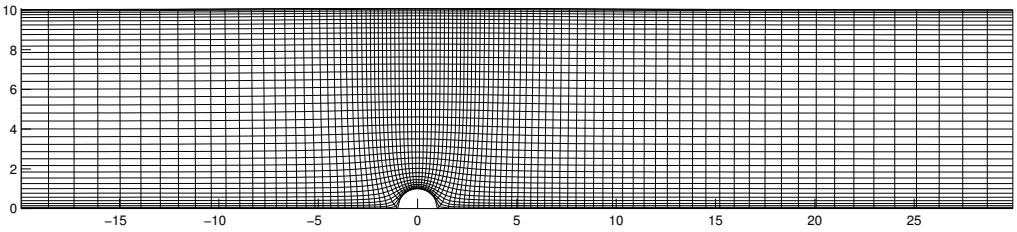

Figure 12.4: Rectangular grid mapped back to the physical Z plane

As we can see the stretchings used in the rectangular grid correspond to a better resolution close to the obstacle and a lower resolution on the regions of low gradients. Also note that the graphs of the grids shown in this section are scaled in both axes to present the features of the different shapes that we will explore, but the solutions were in many cases obtained from grids of larger regions in the physical domain.

With this map we were able to validate the implementation by checking with the previous results obtained using the conformal map proposed by Fornberg. The results from this map were in accordance with those shown in chapter 10 and this was also a good indication that our solution did not have any grid dependence; not only different grid densities were used, but also a different conformal map with a completely different stretching, and no difference was observed in any of the features of the flow. After this validation, let us attack more general geometries by implementing the Joukowski transformation once again, but now to the circle in the Z plane. This time we will use a more general version of the Joukowski map,

$$Z_2 = Z + \frac{\lambda^2}{Z} \quad . \tag{12.3}$$

As we already discussed, for $\lambda = 1 = R$ this map would transform the circle with radius $R = 1$ centered at the origin to the strip from -2 to 2 in the x axis. Now we will use this map to transform the outside of the circle, by first displacing the center

of the circle to have coordinates $(-x_c, 0)$ and letting $\lambda = R - x_c$ [24]. This new map will transform the displaced circle to a symmetric airfoil, whose shape will depend on the parameter x_c and hence on λ.

We will now explore different shapes for different values of x_c. In each case, the resulting airfoils were thinner than the original circle, that is, a more *streamlined* shape with a cross section less than that of the circle. However, as we discussed in page 18, the Reynolds number depends on the size of the obstacle, therefore in each of the cases shown below, the shape was normalized to have cross section equal to 1 in order to be able to compare the results with those of the circle of radius 1 at the corresponding Reynolds number.

12.1 Case $x_c = 0.5$

The sequence of transformations applied to rectangular grid shown in Fig. 12.3 is the following:

$$X = \frac{Z \pm \sqrt{Z^2 - 4}}{2} \quad \text{Inverse Joukowski,}$$

followed by the displacement

$$Z_2 = X - x_c \quad \text{shift the unit circle } x_c \text{ units to the left.}$$

Then

$$Z_3 = Z_2 + \frac{\lambda^2}{Z_2} \quad \text{Where } \lambda = 1 - x_c.$$

Which after scaling to have cross section equal to 1, results in the following grid:

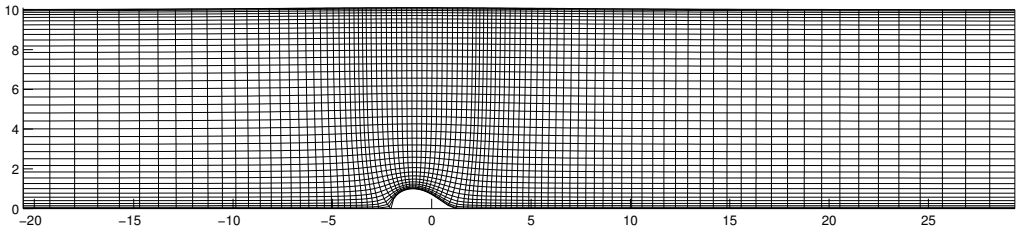

Figure 12.5: Rectangular grid mapped back to the physical Z plane

As mentioned in Chapter 9, the robustness of the design of the program allows us to implement these new geometries by simply replacing elements in the boundary matrix with the corresponding type of boundary. With these new values in the boundary matrix, the program generates a new initial guess, and the function as well the Jacobian will be calculated accordingly for the new set of boundary conditions. The new boundary conditions are defined under the same considerations as before: symmetry, non-slip, far flow and even the non-local boundary condition was used to define the boundary condition for the top without imposing a fixed value like potential flow, that would at some point restrict the growth of the wake bubble. Let us now explore the impact of this more streamlined geometry on the steady solution. Recall

from Fig. 10.5 that the flow starts detaching from the obstacle even for low Reynolds numbers; now observe the behavior of the solution at comparable values of Re:

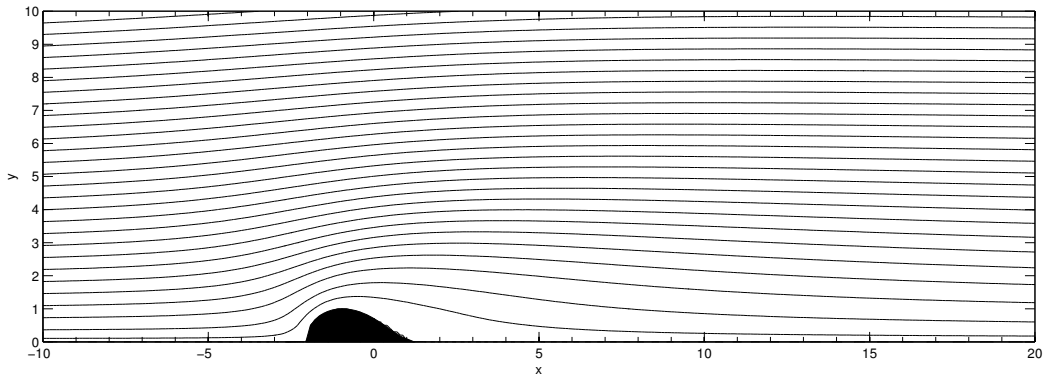

Figure 12.6: Stream Function for Joukowski airfoil with $x_c = 0.5$ at Re=15

With corresponding vorticity

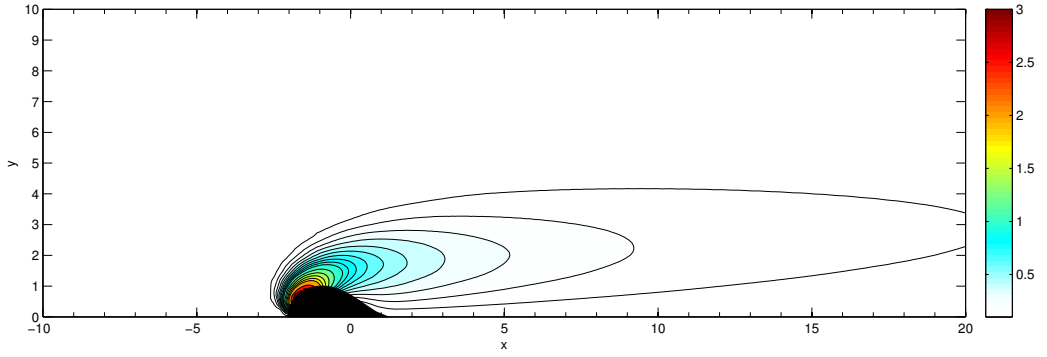

Figure 12.7: Vorticity for Joukowski airfoil with $x_c = 0.5$ at Re=15

In this case there is no separation at low Reynolds numbers, and although the

vorticity in the front of the obstacle is very similar to that of the circular cylinder, the elongated tail does not give rise to the negative vorticity that is generated at posterior region of the obstacle in the circular case as shown in Fig. 10.7. The separation will begin at higher Reynolds numbers, in this case at Re=25 the recirculation region is similar in size to that of the circular case at Re=15. The size of the wake bubble will be in general smaller than that of the circular cylinder for corresponding Re, but it will keep increasing in a similar way:

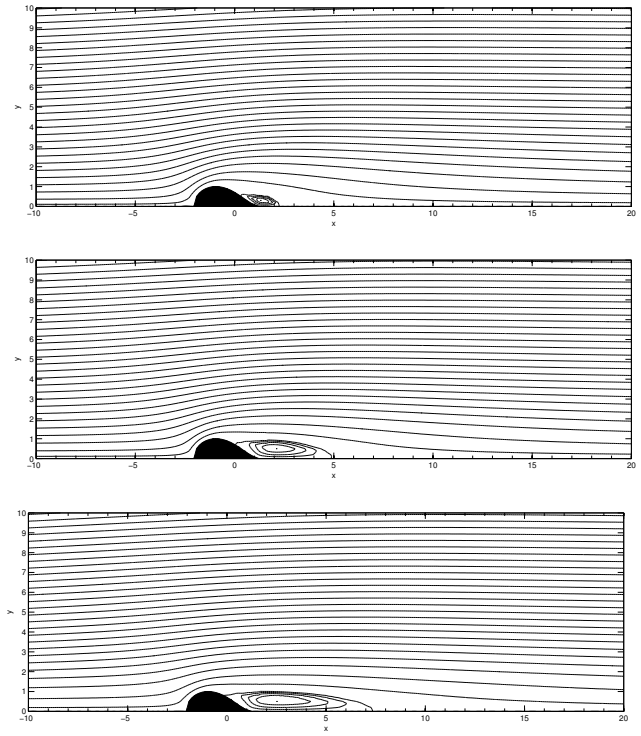

Figure 12.8: Stream Function for Joukowski airfoil with $x_c = 0.5$

12.2 Case $x_c = 0.25$

If we change the parameter to generate a more streamlined obstacle, the Reynolds number required to generate separation of the fluid will increase:

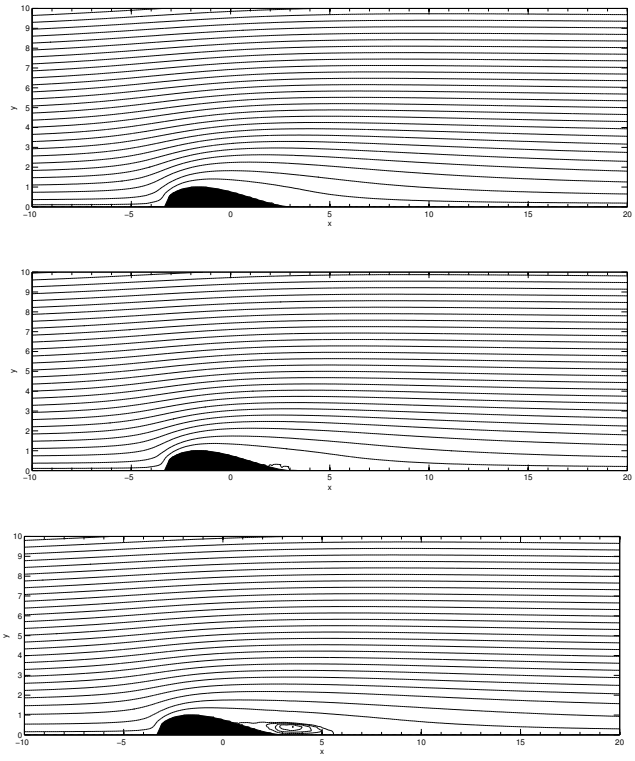

Figure 12.9: Stream Function for Joukowski airfoil with $x_c = 0.25$

As we can see, for Reynolds number 50 the flow shows a very small region of separation close to the end of the tail, compared with the wake in Fig. 12.8, and even for Re=100 the size of the wake is greatly reduced. The reason we always consider flow separation is its impact on the stability of the flow, notions that will be explored

in detail in the next chapter.

12.3 Case $x_c = 0.5$ for inverted airfoil

We can now explore the intuitive idea of considering an obstacle that is not blunt anymore, that is, an object that is sharper in the region facing the incoming flow. This geometry can be easily achieved by displacing the unit circle in the opposite direction compared to our previous case. By shifting the center of the circle to $(x_c, 0)$ and again letting $\lambda = R - x_c$, the map given by 12.3 will generate a symmetric Joukowski airfoil whose shape is the reflection along the y axis of the cases shown above:

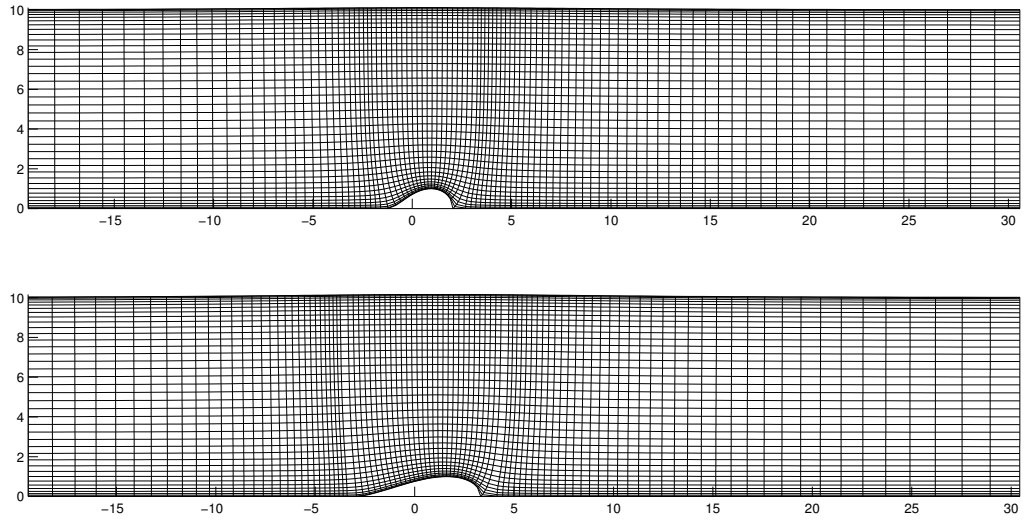

Figure 12.10: Inverted Symmetric Joukowsky airfoils for $x_c = 0.5$ (top) and $x_c = 0.25$ (bottom)

For both of this cases, even though the shape is sharp in the front, its non-streamlined region in the back produced flow detachment:

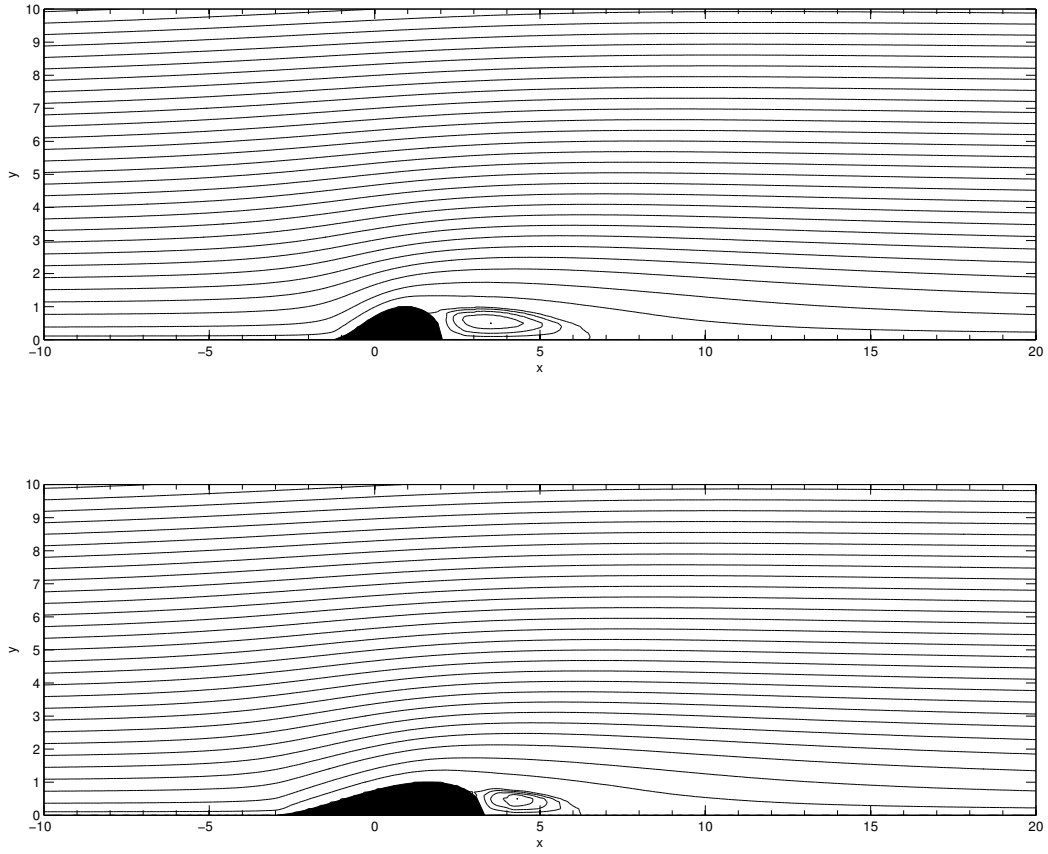

Figure 12.11: Stream lines at $Re = 50$ for $x_c = 0.5$ (top) and $x_c = 0.25$ (bottom)

With corresponding vorticity

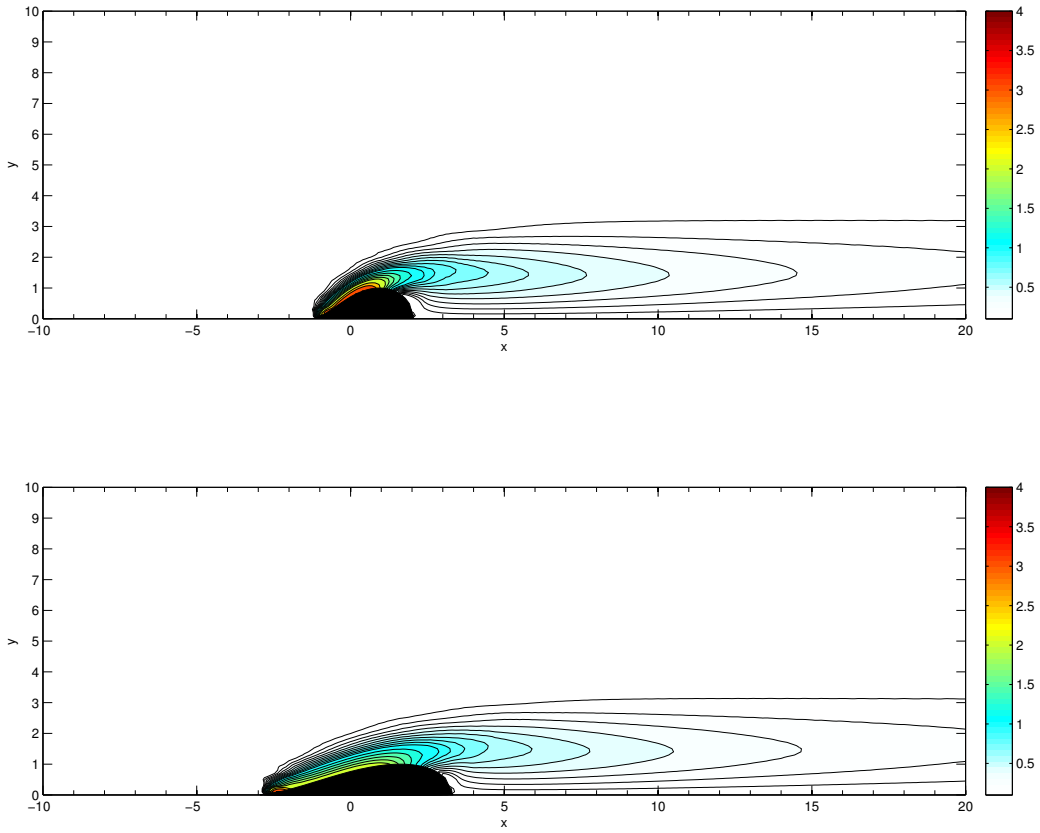

Figure 12.12: Stream lines at $Re = 50$ for $x_c = 0.5$ (top) and $x_c = 0.25$ (bottom)

For the more streamlined version of the airfoil, the vorticity is distributed evenly on the surface compared to the case $x_c = 0.5$ and the only region of high vorticity is in the tip of the airfoil where the flow changes from coming as free flow to a sudden stop at the stagnation point.

Chapter 13

SUCTION BOUNDARY CONDITION

Throughout the project we have discussed flow separation and the creation of the wake bubble; we saw how streamlined obstacles delay the velocity (in terms of increasing Reynolds number) at which the fluid detaches from the surface of the obstacle, but what else can be done to suppress this separation further? One idea is to suck the fluid in the region where the separation appears, and we will approach the problem from a very intuitive point of view.

Flow separation has many implications in practical applications; it can increase drag, and leads in many cases to turbulence, which is out of the scope of this study.

Practical solutions to this problem have been designed before, as is the case of including small orifices in the wings of airplanes to suck air and delay separation. We will study how to model this mathematically from a very basic perspective. I refer to it as *basic* perspective because different studies describe this suction in terms of changes of the vorticity in the surface of the obstacle, again due to the inconvenience of not having a boundary condition for the vorticity in the obstacle. However, as we explained before, the system is complete even if we don't have a boundary condition for the vorticity as long as we have two boundary conditions. In this case both boundary conditions will be for the stream function, not as $\psi = 0$ and $\frac{\partial \psi}{\partial \eta} = 0$ (no-slip boundary condition) but replacing the first by a condition that describes flow going inside of the obstacle.

Recall from 3.6 that for cartesian coordinates

$$u = \frac{\partial \psi}{\partial y} \qquad ; \qquad v = -\frac{\partial \psi}{\partial x} \quad ,$$

then while the no-slip boundary condition $\frac{\partial \psi}{\partial \eta} = 0$ expresses that the tangential velocity in the surface of the obstacle is zero, assigning a value to $\frac{\partial \psi}{\partial \xi}$ would represent a flow inward or outward from the obstacle. In this case while keeping the same boundary conditions as before for the frontal part of the circular cylinder, we will replace the boundary condition for the region where separation starts to occur by

$$\frac{\partial \psi}{\partial \xi} = K_{suction} \quad , \tag{13.1}$$

where $K_{suction}$ will be a parameter that we will control and it will represent the velocity at which the flow is going inside the obstacle. We will use as base for comparison, the flow at Re=25:

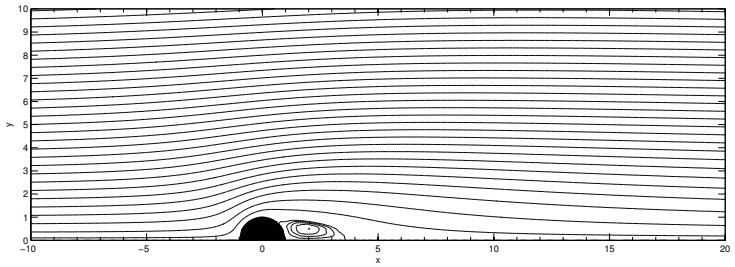

Figure 13.1: Stream function for Re=25

For $K_{suction} = 10$ the separation is almost completely suppressed and for $K_{suction} = 20$ the suction is strong enough to take the streamlines to the inside of the cylinder:

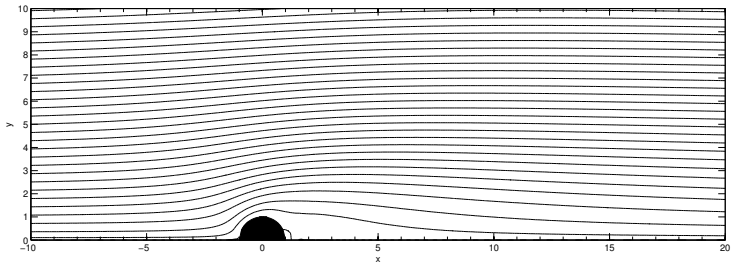

Figure 13.2: Stream function for Re=25, $K_{suction} = 10$

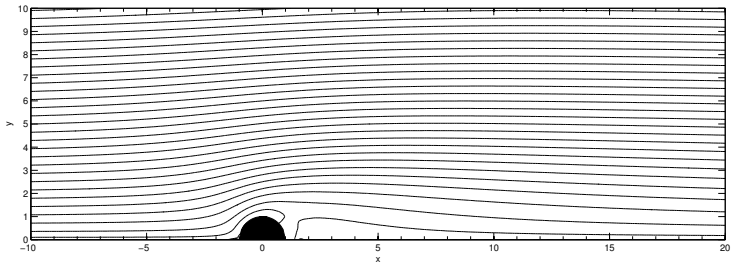

Figure 13.3: Stream function for Re=25, $K_{suction} = 20$

If we keep increasing the suction, more streamlines will get trapped by the obstacle

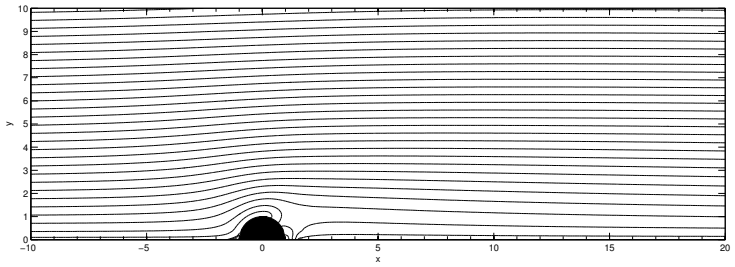

Figure 13.4: Stream function for Re=25, $K_{suction} = 80$

On the other hand, as an experiment, if $K_{suction}$ takes a negative value, we would be blowing fluid instead of absorbing it, in that case the wake would actually increase in size.

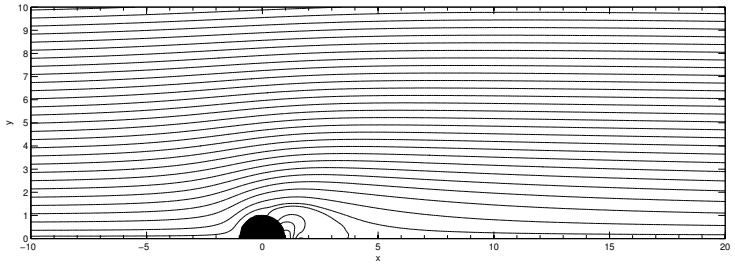

Figure 13.5: Stream function for Re=25, $K_{suction} = -80$

Chapter 14

CONCLUSIONS

We successfully implemented spectral methods to solve the Navier-Stokes equations for a viscous flow past different geometries. The methods used were tested and showed no grid dependence, not only by changing grid densities but also by using different conformal maps.

Even though a grid of 40×160 was used to reach Reynolds number 550, the power of spectral accuracy allowed us to calculate solutions with an error of $\epsilon = O(10^{-12})$ for grids with only 20 points in the η direction. The threshold for considering convergence of the Newton's Method was $\epsilon < 10^{-11}$, which was sometimes attained after only 5 to 6 iterations even for discretizations with 20 points in the direction where spectral methods were used. For a discretization of 20×100 the equations were solved in 32.52

seconds, requiring 8 iterations to achieve convergence ($\epsilon = 5.68 \times 10^{-12}$) on an Intel Core(TM)2 Duo CPU T6400 at 2.00GHz, with 4GB Ram and 4GB of Readyboost as pagefile. We can compare this performance with SOR method with second order finite differences on a 60×100 which required a vast amount of 4650 iterations due to the very small relaxation parameter required to avoid spurious artificial time instabilities from developing. These 4.6 thousand iterations only required 34.5 seconds (on the same computer) which is comparable to our previous results, but the accuracy was only $\epsilon = 10^{-4}$ compared with $\epsilon = 5.68 \times 10^{-12}$ from spectral methods.

In terms of accuracy, spectral differentiation with Newton's Method is clearly more powerful, however as we can see, the computational cost increases very fast for finer grids. For this specific example, in the case of Newton's method, we solved a system of 4000 equations with 4000 unknowns (a 20×100 grid for both stream and vorticity) where the Jacobian is not as sparse as the case of Finite differences due to the full matrices from spectral differentiation. This structure is definitely a limiting factor when trying to solve the system on larger matrices. For Reynolds numbers close to 550 we required a grid with a size of 40×160, and at this point we were already reaching the limits of the computer power (pagefile use as memory is extremely slow to make it viable for computations). On the other hand, with SOR with finite differences we can increase the number of points in the grid without incurring in memory problems due

to the fact that the process is completely algebraic. Then, we can easily implement grids of sizes like 600×1000 like the ones used in [12], but at the expense of sacrificing accuracy.

The characteristics of the wake bubble were studied, showing the wake length to increase linearly for low Reynolds numbers (up to Re=130) but changing its behavior as the vorticity gets convected back to the wake bubble. The vorticity in the surface of the obstacle was studied for different Reynolds numbers and was in accordance with results seen in [8](Fig. 12). Drag coefficients were calculated and compared with previous results form Fornberg[8] and Gushchin & Schennikov[19].

With the robust implementation of the method we were able to study the flow past different geometries. Different symmetric Joukousky airfoils were studied as a sample of the broader variety of problems that can be explored by the use of conformal maps and arbitrary mesh densities. As another example of the versatility of the methods, we experimented with suction boundary conditions and the impact on the flow solution. All these explorations gave us the opportunity to show that many of the implementation ideas do not have to be restricted to computational fluid mechanics, they can be easily exported to a larger spectrum of partial differential equations.

APPENDIX

Appendix A

PHYSICAL PROPERTIES OF SOME FLUIDS

Fluid (At atmospheric pressure)	**T**[°C]	**Density** ρ $[\frac{kg}{m^3}]$	**Viscosity** ν $[\frac{kg}{ms}]$
Water	0	999.9	1.787×10^{-3}
	10	999.7	1.304×10^{-3}
	20	998.2	1.002×10^{-3}
	40	992.3	6.54×10^{-4}
	60	983.2	4.67×10^{-4}
	80	971.8	3.55×10^{-4}
	100	958.4	2.83×10^{-4}
Air	-100	2.040	1.16×10^{-5}
	0	1.293	1.71×10^{-5}
	50	1.093	1.95×10^{-5}
	100	0.946	2.18×10^{-5}
	500	0.456	3.58×10^{-5}
	1000	0.277	4.82×10^{-5}
Motor Oil(SAE 10)	30	~ 875.2	0.2
Glycerine	0	~ 1173	10.000

BIBLIOGRAPHY

Bibliography

[1] S. Koonin, D. Meredith, *Computational Physics*, FORTRAN Version.

[2] John C. Tannehill, Dale A. Anderson, Richard H. Pletcher, *Computational Fluid Mechanics and Heat Transfer*, 1997 Second Edition.

[3] M. Griebel, T. Dornseifer, T. Neunhoeffer, *Numerical Simulation in Fluid Dynamics: A Practical Introduction*, SIAM Monographs on Mathematical Modeling and Computation.

[4] L. D. Landau and E. M. Lifshitz, *Fluid Mechanics*, Editorial Revert 1986.

[5] H. Schlichting, *Boundary-Layer Theory*, McGraw-Hill Book Co. New York 1968.

[6] G. K. Batchelor, *A proposal concerning laminar wakes behind bluff bodies at large Reynolds number*, Journal of Fluid Mechanics, 1 (1956), 388

[7] B. Fornberg, *Computing Steady Incompresible Flows past Blunt Bodies A Historical Overview*

[8] B. Fornberg, *Steady Viscous Flow Past a Circular Cylinder up to Reynolds Number 600*, Journal of Computational Physics 61, 297-320 (1985)

[9] B. Fornberg, *Steady Viscous Flow Past a Sphere at High Reynolds Numbers*, Journal of Fluid Mechanics (1988), vol. 190, pp. 471-489

[10] B. Fornberg, *Steady Incompresible Flow Past a Row of Circular Cylinders*,

Journal of Fluid Mechanics (1991), vol. 225, pp. 655-671

[11] Maurice Roy, *Mcanique. Milieux Continus*,Chapitre 3 Mcanique des fluides

[12] German A. Vargas, *Steady Solution of The Navier-Stokes Equations for a Viscous Flow Past a Circular Cylinder*. Wichita State University (2004)

[13] Lloyd N. Trefethen, *Spectral Methods in MATLAB*, Society for Industrial and Applied Mathematics (2000)

[14] B. Fornberg, *A Practical Guide to Pseudospectral Methods*, Cambridge University Press (1996)

[15] T. Davis, *Direct Methods for Sparse Linear Systems: the CXSparse package*, http://www.cise.ufl.edu/research/sparse/CXSparse/ (date cited: May 2009)

[16] Frederick S. Sherman, *Viscous Flow*, McGraw-Hill Publishing Company

[17] D. Leutloff, R. C. Srivastava (Eds.), *Computational Fluid Dynamics*, Selected Topics, Springer

[18] L. Prandtl, Ph.D. and O. G. Tietjens, Ph.D., *Fundamentals of Hydro- and Aeromechanics*.

[19] V. A. Gushchin and V. V. Schennikov *A numerical Method of solving the Navier-Stokes equations*, (1974)

[20] Leigh Page Ph.D., *Tratado de Fsica Terica*,Segunda Parte. Hidrodinmica

[21] W. F. Hughes, J. A. Brighton, *Theory and Problems of Fluid Dynamics*, Second Edition

[22] Paul. A Tipler, *Physics for scientist and engineers* Fourth Edition, W.H Freeman and Company/Worth Publishers

[23] FORTRAN POWER STATION, *Reference*

[24] *The Joukowski Transformation*,
http://www.diam.unige.it/∼irro/conformi_e.html (date cited: May 2009)

[25] *Computational Fluid Dynamics, CFD, Modeling*,
http://www.alentecinc.com/dem.htm (date cited: May 2009)

[26] *FORTRAN LIB Free Software*,
http://www.fortranlib.com/freesoft.htm (date cited: May 2009)